

Accepted for publication in The Astronomical Journal

The Solar Neighborhood *XXVIII*: The Multiplicity Fraction of Nearby Stars from 5 to 70 AU and the Brown Dwarf Desert Around M Dwarfs

Sergio B. Dieterich, Todd J. Henry

Georgia State University, Atlanta, GA 30302-4106

dieterich@chara.gsu.edu

David A. Golimowski

Space Telescope Science Institute, Baltimore, MD 21218

John E. Krist

Jet Propulsion Laboratory, Pasadena, CA 91109

Angelle M. Tanner

Mississippi State University, Starkville, MS 39762

ABSTRACT

We report on our analysis of *HST/NICMOS* snapshot high resolution images of 255 stars in 201 systems within ~ 10 parsecs of the Sun. Photometry was obtained through filters *F110W*, *F180M*, *F207M*, and *F222M* using *NICMOS* Camera 2. These filters were selected to permit clear identification of cool brown dwarfs through methane contrast imaging. With a plate scale of 76 mas/pixel , *NICMOS* can easily resolve binaries with sub-arcsecond separations in the $19''.5 \times 19''.5$ field of view. We previously reported five companions to nearby M and L dwarfs from this search. No new companions were discovered during the second phase of data analysis presented here, confirming that stellar/substellar binaries are rare. We establish magnitude and separation limits for which companions can be ruled out for each star in the sample, and then perform a comprehensive sensitivity and completeness analysis for the subsample of 138 M dwarfs in 126 systems. We calculate a multiplicity fraction of $0.0_{-0.0}^{+3.5}\%$ for L companions to M dwarfs in the separation range of 5 to 70 AU, and $2.3_{-0.7}^{+5.0}\%$

for L and T companions to M dwarfs in the separation range of 10 to 70 AU. We also discuss trends in the color-magnitude diagrams using various color combinations and present astrometry for 19 multiple systems in our sample. Considering these results and results from several other studies, we argue that the so-called “brown dwarf desert” extends to binary systems with low mass primaries and is largely independent of primary mass, mass ratio, and separations. While focusing on companion properties, we discuss how the qualitative agreement between observed companion mass functions and initial mass functions suggests that the paucity of brown dwarfs in either population may be due to a common cause and not due to binary formation mechanisms.

Subject headings: binaries: close — infrared: stars — stars: brown dwarfs, low mass, solar neighborhood, statistics

1. Introduction

The mass function, multiplicity fraction, and the mass-luminosity relation are three of the most important characteristics of a stellar or substellar population. However, all three remain poorly constrained for Very Low Mass (VLM) stars. Although the lowest mass stars, the M dwarfs, dominate the Galaxy in numbers and comprise the majority of our stellar neighbors (Henry et al. 2006), not a single M dwarf is visible to the naked eye. Over the last two decades, advances in observational astronomy have made a thorough study of these faint stars possible. Empirical mass-luminosity relations (Henry & McCarthy 1993; Henry et al. 1999; Delfosse et al. 2000) have achieved a high degree of reliability for early to mid M dwarfs, with progress continuing for later M dwarfs at the end of the main sequence. Large sky surveys such as the 2 Micron All Sky Survey (*2MASS*) in the near infrared (Skrutskie et al. 2006) and the Sloan Digital Sky Survey (*SDSS*) in the optical (York et al. 2000) have provided a wealth of new data for population studies, but lack the angular resolution necessary to investigate the Multiplicity Fraction (MF) and Companion Mass Function (CMF) at separations corresponding to the short periods necessary for determining dynamical masses.

The discovery of GJ 229B, the first unequivocal brown dwarf (Nakajima et al. 1995), followed by hundreds of others¹, raised fundamental questions about our understanding of low mass star formation. Are VLM stars and brown dwarfs products of a single mechanism of (sub)stellar formation applicable to a wide range of masses? Or, do brown dwarfs

¹A current list of known L and T dwarfs is maintained at www.dwarffarchives.org.

constitute a fundamentally different population? Does the trend in the stellar mass function producing more stars at lower masses continue into the brown dwarf regime, therefore making them more numerous than their stellar cousins? What do multiplicity properties, such as the overall multiplicity fraction and the separation distribution, tell us about the environments in which VLM stars and brown dwarfs were born? These are some of the fundamental questions that have only recently been addressed through a combination of sky surveys (e.g., Bochanski et al. 2010), wide separation common proper motion searches (e.g., Allen et al. 2007; Allen & Reid 2008), high resolution multiplicity surveys (e.g., Reid & Gizis 1997; Close et al. 2003; Gizis et al. 2003; Lowrance et al. 2005; Reid et al. 2008; Metchev & Hillenbrand 2009) and the establishment of trigonometric parallaxes for a large sample of objects (e.g., Dahn et al. 2002; Henry et al. 2006)

Thorough characterization of any stellar population requires the study of a volume limited sample. In an effort to better understand these properties, we have conducted an *HST/NICMOS* snapshot program imaging 255 objects in 201 star systems with trigonometric parallaxes placing them within ~ 10 pc of the Sun (Table 1). We used the technique of methane imaging (Rosenthal et al. 1996; Tinney et al. 2005) to clearly distinguish cool brown dwarf companions. In 2004 we reported the detection of four M dwarf companions and one binary L dwarf in a triple system (Golimowski et al. 2004b, hereafter G04). With small infrared contrasts ranging from ~ 0 magnitudes (GJ 1001BC) to 4.5 magnitudes (GJ 84AB), the companions we reported in 2004 were relatively bright. We have since carried out a deeper search of the data, establishing formal sensitivity limits for the detection of companions in the field of each primary target and extending the limiting magnitude differences routinely to 11 at separations of $3''0$, 8 at $1''0$, 4 at $0''4$, and 2 at $0''2$ (§5.3, Figure 6a). Having completed the deeper search of the data with no further detections, we now report on the magnitude and separation limits to which we can rule out companions for each object in our sample. We also discuss what the lack of additional brown dwarf detections tells us about the multiplicity fraction of systems with VLM secondaries in these mass and separation regimes.

We describe the general characteristics of our sample and discuss how the observed sample relates to our current knowledge of the solar neighborhood in §2. Instrumental aspects of the observations relevant to obtaining our sensitivity limits are briefly reviewed in §3, and a detailed discussion of our Point Spread Function (PSF) insertion method for testing the sensitivity of the search is given in §4. We discuss photometric trends in our color system and note several benchmark objects in §5.1. We report new astrometric data for 19 known binary systems in §5.2, and discuss the sensitivity of the search in §5.3. In §5.4 we establish a sub-sample of 126 M dwarf systems for which we calculate the multiplicity fraction, including substellar companions, from 5 to 70 AU based on companion detections (or lack thereof) and completeness arguments. We discuss what our results mean in the

context of the “brown dwarf desert” in §6.1 and §6.2. Finally, we end by comparing young cluster multiplicity studies, estimates of the Galactic disk luminosity function, and our results in §6.3, and summarize our conclusions in §7.

2. General Characteristics of the Sample

Our target list was designed to provide a sample that is representative of the solar neighborhood. Because this survey was an *HST* snapshot program, our targets were pulled from a large pool of selected targets in order to fill small gaps in *HST*’s observing schedule. The REsearch Consortium on Nearby Stars (*RECONS*)² is engaged in an effort to obtain a census and thorough characterization of the population of stars within 25 pc of the Sun, with a particular concentration on stars closer than 10 pc (Henry et al. 2006). In order to be a member of the *RECONS* 10 pc sample, an object must have a trigonometric parallax greater than 100 mas, with an error smaller than 10 mas. We used the *RECONS* 10 pc sample as a starting list for our search and allowed the *HST* snapshot scheduling process to effectively select a random subsample from the 10 pc sample. Table 1 summarizes several tallies of the observed sample. These observations comprise 69% of the *RECONS* 10 pc sample (epoch 2012.0), including main sequence stars, white dwarfs, L and T dwarfs, but excluding extrasolar planets. We note that because trigonometric parallaxes for nearby stars are constantly being updated, 17 objects in 13 systems originally included in our search are no longer members of the 10 pc sample. We still include their data as individual stars in this paper, but exclude them from statistical considerations in order to keep the sample volume limited.

Figure 1 shows the spectral type distribution of the *NICMOS* snapshot sample. Out of the 218 resolved objects within 10 pc we observed, 138, or 63%, are M dwarfs. This number is a very close match to the M dwarf fraction in the *RECONS* 10 pc sample, which is 248 out of 357 objects, or 69% (epoch 2012.0). The preponderance of M dwarfs in our sample means that even though the sample is a random representation of the solar neighborhood, it focuses on the spectral type that is least scrutinized by RV companion searches and open cluster imaging searches. By studying nearby M dwarfs, which comprise a disk rather than cluster population, we are mapping the brown dwarf desert in a largely unexplored region.

²Information about *RECONS* and periodically updated versions of the 10 pc census are available at www.recons.org.

3. Observations and Data Reduction

G04 describe technical aspects of the observations in detail. We give a brief summary here and highlight the aspects that are most relevant in achieving the sensitivities we later quote for each individual target.

We obtained direct images of each target using *NICMOS* Camera 2 (*NIC2*) through four near infrared filters during cycles 7 (1997–1998) and 11 (2002–2003). *NIC2* has a plate scale of $0''.076 \text{ pixel}^{-1}$ and a field of view of $19''.5 \times 19''.5$ (Viana et al. 2009, Thatte et al. 2009)³. Targets were imaged through the *F110W*, *F180M*, *F207M*, and *F222M* filters, centered at $1.10 \mu\text{m}$, $1.80 \mu\text{m}$, $2.07 \mu\text{m}$, and $2.22 \mu\text{m}$, respectively. Because *HST* observations are not subject to atmospheric absorption, the *NICMOS* filters are not defined to sample atmospheric transmission windows in the way that ground based near infrared filters are. The resulting filter set is non-standard when compared to ground based systems, but allows the user to construct a color scheme that is more suitable for the underlying physics being investigated. Figure 2 shows the transmission curves for the selected *NICMOS* filters, with the *2MASS* *J*, *H*, and *K_S* filters also plotted for comparison. The four filters in this survey were selected to detect the strong CH_4 absorption bands observed in T dwarf spectra at $1.7 \mu\text{m}$ and $2.2 \mu\text{m}$, in effect imaging in and out of these absorption bands. Depending on the filter choice, there is a drastic color shift of up to three magnitudes for T dwarfs. A late T dwarf appears blue in *F110W*–*F180M* (0.0 to -1.0 , Figure 3a) whereas it is red in *F180M*–*F207M* (1.0 to 2.0, Figure 3c). Because no background source is likely to have such a strong color shift, T dwarfs are readily identified in this color scheme. This technique is commonly known as methane imaging and has been used to successfully identify brown dwarfs in photometric observations (Rosenthal et al. 1996; Tinney et al. 2005).

By centering the targets on the detector, we searched for companions within a radius of $9''.5$, except for a small ($\sim 1''$ in diameter) artifact due to the coronagraphic hole on the upper left quadrant of the detector⁴. A few targets had large coordinate uncertainties, in most cases due to poorly constrained high proper motions. These targets were not properly centered in the field of view, and are specified in the notes to Table 2. Although some of our primary targets are very bright (e.g. Sirius, Vega, Procyon), we did not use the coronagraph because it would make the acquisition process too long for a snapshot program and its peripheral

³ *HST/NICMOS* documentation, including the *NICMOS Instrument Handbook* and the *NICMOS Data Handbook*, is currently available from the Space Telescope Science Institute at www.stsci.edu/hst/nicmos

⁴ *HST*'s roll orientation during a given exposure is constrained by the need to keep the solar arrays facing the Sun. Consequently, the position angle of the coronagraphic hole with respect to celestial north, as well as the image's overall orientation, varies widely among the images of our targets.

position in the detector would severely limit our search radius. Placing the primary target behind the coronagraph would also add uncertainty to the measurement of the position angle and separation of any binary systems. Even with saturated central targets, we could still search for companions, albeit with a lower sensitivity closer to the central target (Table 2).

We coadded two sets of exposures for each target, resulting in a total exposure time of 64s for the *F110W* and *F180M* filters and 128s for the *F207M* and *F222M* filters. Saturation of bright targets and cosmic ray hits were minimized by using *NICMOS*'s multi-accumulate (*MULTIACCUM*) mode, which reads the detector in a non-destructive manner at predetermined time intervals. In the event of saturation or a cosmic ray hit, the *NICMOS* pipeline scales the value from unaffected readouts so as to obtain the approximate value due to the astronomical source. Only pixels that saturate or are hit by a cosmic ray before the first readout at 0.303 s are lost. For targets that were bright enough to saturate during the first readout, we obtained photometry by using PSF fits.

Because there is no background atmospheric glow, the extended PSF of the primary target is the dominant source of background flux obscuring any fainter objects in the field of view. We subtracted a properly scaled PSF of another star of similar spectral type and brightness from the survey from the PSF of each target. A detailed discussion of the PSF subtraction process is given in Krist et al. (1998, hereafter K98). The quality of the subtraction varied from target to target and depends primarily on whether or not a good PSF match could be obtained. The PSF varies with target color, telescope focus, and the position of the *NICMOS* cold mask (K98). We were always able to find an isolated star whose PSF was used as the reference for PSF subtraction. If the PSF reference had been a close binary or if it had been contaminated by background sources, we would have noticed a physically unrealistic negative PSF in the subtracted image. We then performed aperture photometry on the primary target as well as any other sources in the field of view using standard IRAF routines and the aperture corrections for encircled energy fraction listed in Table 2 of K98. To verify the validity of the aperture corrections, we performed the photometry of the crowded field of LHS 288 (31 sources, Figure 4), varying the aperture from three to six pixels ($0''.23$ to $0''.46$). The photometry agreed to $\lesssim 0.03$ magnitudes in all bands, regardless of aperture. For the final photometry we chose a six pixel aperture, except in cases when a crowded field or a source near the edge of the field required a smaller aperture.

4. Determining the Sensitivity of the Search

We define the “sensitivity” of the search as the extent to which we can detect or rule out the existence of a companion to a given star at a given separation and image contrast

Δm . The sensitivity varies from target to target and is influenced by the overall brightness of the primary target, the quality of the PSF subtraction, the image filter, intrinsic detector noise, and the prominence of detector artifacts. For each image these factors interact in a complex way, thus making it difficult to draw generalizations about instrumental sensitivity for the survey as a whole. We have therefore devised a method to measure the sensitivity achieved for each target at various separations, and quote individual results in Table 2.

Because *HST* is not subject to atmospheric effects, its images are inherently stable, thus facilitating PSF modeling. We used *Tiny Tim 6.3* (Krist & Hook 1997) to simulate generic *NIC2* stellar PSFs through the four filters used in the search. The properly scaled model PSFs were inserted into the PSF subtracted images of the primary targets to test our ability to detect companions at a range of contrasts and separations using a customized *IDL* code. At sub-arcsecond separations, we inserted a single companion at separations of $0''.2$, $0''.4$, $0''.6$, and $0''.8$ and a varying range of contrasts at random position angles (Figure 5a). The PSF insertion code automatically excluded the strong diffraction spikes present in well-exposed *NICMOS* images at 45° , 135° , 225° , and 315° . The residual flux from the PSF subtracted primary target was set to zero at a radius interior to the position of the artificially inserted companion to facilitate visual inspection. At separations of $1''.0$ or greater, we produced an image where artificial companions were arranged in a radial pattern around the PSF subtracted primary (Figure 5b). This pattern tested the sensitivity at separations of $1''.0$, $2''.0$, $3''.0$, and $4''.0$ at contrasts typically incremented from 6 to 13 magnitudes. The simulated images and their surface plots were then visually inspected. In both regimes, an artificially inserted companion was considered detectable if it was visible in the simulated image and if a surface plot around the companion indicated that the artificial PSF retained its characteristic stellar shape, with its peak clearly above the background noise, corresponding to a typical signal-to-noise of 3–5. Although automating the PSF recovery process (e.g., by using a cross-correlation algorithm) would have saved a considerable amount of time, we were not convinced that automated methods would appropriately distinguish between real astronomical sources and residuals of the central star’s PSF subtraction, which can at times mimic star-like profiles.

5. Results

Other than the five companions reported in G04, which focused on individual discoveries, we detected no further new companions during this second phase of our search. We now report on the photometry, astrometry, and search sensitivities attained during the survey. With a statistically robust sample of 255 stars surveyed, these results allow us to make

assessments of the multiplicity of stars in the solar neighborhood from a stellar population perspective.

5.1. Color-Magnitude Diagrams

We constructed color-magnitude diagrams for the twenty-four different color-magnitude combinations from our observations through the four filters. Because our sample includes only four certain substellar objects (GJ 1001 B and C, GJ 229B, and 2MASSI J0559191-140448), we used synthetic photometry from the spectra of known L and T dwarfs to better determine the form of the substellar sequence in this color space. These values were obtained using flux-calibrated, near infrared spectra (Geballe et al. 2002; Knapp et al. 2004), weighted mean trigonometric parallaxes (Golimowski et al. 2004b, and references therein), and the *NICMOS* Exposure Time Calculator produced by STScI. Figure 3 shows four color-magnitude diagrams that are particularly well suited for mapping the stellar and substellar main sequence. Main sequence targets and the thirteen white dwarfs in the survey are labeled with large dots. In these diagrams, we initially assume that any object in the field of view of a primary target is a companion and therefore shares the primary’s trigonometric parallax. If the assumption is correct, the object will fall within the stellar or substellar sequence. Background objects, labeled with small dots, appear as having unrealistically faint absolute magnitudes and tend to cluster at the bottom of the diagrams.

The trends in the $F110W-F180M$ and the $F110W-F222W$ colors (Figures 3a and 3b) clearly indicate that the onset of CH_4 absorption happens sharply around the L6 spectral type, where the colors turn blue. Although any single diagram may show an overlap between the substellar sequence and the brighter background objects, the degeneracy is broken when we consider that L and T dwarfs follow different trends from the background sources in different color combinations. The most dramatic example of these shifts appears in Figures 3c and 3d, where methane imaging causes a large shift from blue to red for the T dwarfs while the background sources show little change.

5.1.1. Benchmark Objects

GJ 1245ABC (labels 1, 2, and 4 in Figure 3) is an interesting system containing three low mass components. In particular, GJ 1245C (4) is one of the latest M dwarfs for which a dynamical mass is known. With a mass of $0.074 \pm 0.013 M_\odot$ (Henry et al. 1999), this object lies close to the theoretical hydrogen burning mass limit.

G 239-25B (label 3) was discovered during the first phase of this search, and the implications of the multiplicity of the G239-25 system are discussed in G04. Forveille et al. (2004) assign it a spectral type of $L0\pm 1$ based on near infrared spectra. This spectral classification makes G 239-25B an important benchmark of the M/L transition at the bottom of the main sequence. Its proximity in color space to GJ 1245C re-enforces the importance of both objects as benchmarks.

GJ 1001BC (labels 5, 6, and 7) was resolved as a double L4.5 dwarf, and is discussed in detail in G04. The components of the system are nearly equal in luminosity, and we plot them both individually (6 and 7) and combined (5) to illustrate how an equal flux binary appears in the sequence. When compared to the L/T sequence outlined by the synthetic photometry, both components of GJ 1001BC lie just before the strong shift towards the blue that happens as a result of the onset of CH_4 absorption. Their positions at this turning point are most easily seen in the $F110W-F222M$ color (Figure 3b). We are currently working to refine the parallax of GJ 1001ABC, and to obtain dynamical masses for the BC pair.

Finally, 2MASSI J0559191-140448 (T4.5, label 8) and GJ 229 B (T6, label 9) are the only T dwarfs imaged in the survey, and serve as confirmations that the sequence outlined by the synthetic photometry agrees with real photometry. Whereas GJ 229B is a companion to the M0.5V dwarf GJ 229A, 2MASSI J0559191-140448 is an isolated brown dwarf. Its positions in panels a and b of Figure 3 illustrate how a mid T dwarf can easily be mistaken for a white dwarf when more color combinations are not used to break the degeneracy.

5.1.2. Background Objects with Companion-Like Colors

Figure 3 shows that there are several sources having colors that mimic the colors of substellar companions in one or more panels. The ambiguity is often accentuated when analyzing data sets with simpler color combinations that were not designed a priori to discriminate substellar objects (e.g. *2MASS JHK_s*). Interstellar reddening considerations are particularly useful in identifying false companions. Because the distance horizon of our search is only ~ 10 pc, any bona fide companions should not have appreciable reddening in the near infrared. Conversely, distant main sequence or giant stars may have significant reddening in the $F110W-F180M$, $F110W-F207M$, and $F110W-F222M$ colors, which may place background objects in the color space occupied by L and T dwarfs. The degeneracy is broken when considering the $F207M-F222M$ and especially the $F180M-F207M$ colors, where the narrow spectral coverage reduces the reddening of distant main sequence sources (Figures 3c and 3d). Table 3 lists cases where the distinction between a background object and a putative companion was particularly subtle based on colors alone. The white dwarfs

as a group mimic late L and early T dwarfs in $F110W-F180M$ and $F207M-F222M$, but the degeneracy is broken in $F180M-F207M$.

5.2. Astrometry of Known Binaries

High resolution images of nearby binary systems present opportunities to map relatively short period orbits and therefore determine dynamical masses. While actual orbital mapping is beyond the scope of this work, we report the astrometry for select systems in Table 4. In order to be listed in Table 4, both components of the system must have been imaged simultaneously in the same *NIC2* field of view, and the centroids must be determined to a precision better than ± 1 pixel. The values we report are the weighted averages of separations and position angles measured from the PSF centroids in all filters for which saturation did not prevent reliable centroiding. In the simplest case of non-saturated and non-overlapping PSF cores, we adopt a centroiding error of ± 0.1 pixel (G04). Twelve out of the 19 pairs listed in Table 4 meet these criteria. The other seven pairs are either very closely separated stars for which the PSF cores overlap significantly or have central pixel saturation. In either case, the centroiding was determined using PSF fits. With the exception of the M dwarfs, the majority of binaries in our survey had their PSF cores saturated beyond the point where we could compute meaningful astrometry. The precise value of the *NICMOS* plate scale varied during HST cycle 7 (1997–1998) due to cryogen expansion that distorted the dewar housing the detectors. To calibrate the plate scales for our observations, we used the values tabulated by the Space Telescope Science Institute based on routine monitoring of crowded star fields. For separations, the errors listed in Table 4 take into account the four centroiding uncertainties (x_a, y_a, x_b, y_b) added in quadrature. For position angles, the errors take into account the propagated centroiding errors.

5.3. Results from the Sensitivity Search

Table 2 lists the faintest detectable absolute magnitudes for putative companions at a range of angular separations from each target star in the survey. The distances and spectral types listed are based on the best trigonometric parallaxes and spectral type estimates available in the literature or unpublished trigonometric parallaxes recently measured or improved by our group. It is important to note that each line in Table 2 shows the results of one PSF insertion simulation, and does not necessarily correspond to a single star. As described in the notes column, a single PSF insertion simulation may have been done around the two components of a resolved system if their separation was small or if their contrast was large

enough for the primary to dominate the field. Because of these situations, the number of entries in Table 2 is not meant to add up to the sample counts in Table 1. The reader is referred to Table 1 for overall statistics of the sample and to Table 2 for data on individual targets.

All targets were inspected for real companions visually in all four bands over the entire field of view. Several factors must be considered when choosing the best filter for the PSF insertion simulations. Out of the four filters used in the search, the *F110W* and *F180M* filters are the most suitable for close separations ($\lesssim 0''.4$) due to their narrower PSFs when compared to the *F207M* and *F222M* filters. Whereas L dwarfs are brighter in *F180M* than in *F110W*, the T dwarfs are much fainter in *F180M* due to methane absorption. Although the *F110W* band produces the narrowest PSFs due to its shorter wavelength and is an intrinsically bright band for T dwarfs, we chose to report the sensitivities in the *F180M* band for two reasons. First, our uniform exposure time scheme (§3) causes brighter targets to saturate out to several pixels in the *F110W* band even in 0.303s, decreasing our ability to probe the smallest separations. Second, the width of the *F110W* PSF is comparable to the *NIC2* pixel scale, causing a sharp spike on the central pixel (K98, Table 2). In low signal-to-noise situations it becomes difficult to distinguish the *F110W* PSF from bad pixels or other sharp artifacts introduced during the PSF subtraction process. As discussed in §5.4.2 our sensitivity limit falls mostly in the L dwarf regime for sub-arcsecond separations, and in the T dwarf regime for wider separations. Based on comparisons in particularly clear images, we estimate that using *F110W* instead of *F180M* would increase our sensitivity by ~ 1 magnitude, but would pose an unacceptable risk of false detections at close separations. We therefore uniformly report sensitivities for all separations in *F180M*, but emphasize that those values can be safely transformed to *F110W* limiting magnitudes for separation greater than $1''.0$ by adding 1.0 magnitude to the *F180M* limits in Table 2. Because late T dwarfs appear the faintest in *F180M*, a detection in that band also implies detection in the other three bands, therefore providing the color information needed to characterize the object. Listing our simulation results in the *F180M* band therefore maximizes the instrumental dynamic range of the images while still providing the sensitivity needed to characterize T dwarfs.

5.4. The M Dwarfs

Of the 188 star systems imaged within 10 pc in this survey, 126 systems have M dwarfs as the primary (or single) component⁵. Because these M dwarfs were selected randomly from a volume limited sample based on their trigonometric parallaxes, the sub-sample lends itself well to statistical considerations. We now apply the sensitivity limits in Table 2 to derive the multiplicity fraction for M dwarfs under several scenarios.

5.4.1. Establishing Search Completeness for M Dwarfs

Figures 6 a and b show the ranges in sensitivities obtained for M dwarfs at each of the eight angular separations probed by the PSF insertion simulations. In Figure 6b, we used the known distance to each target to convert contrasts into absolute magnitudes, and relate these absolute magnitudes to the spectral types of putative companions. Because sensitivity is a complex function of contrast, instrumental background, apparent magnitude, and the quality of the PSF subtraction, there is a significant spread about the mean values quoted in Figure 6. Overall, we would detect companions with $\Delta F180M=2.5$ to 10.2 magnitudes at separations of $0''.2$ to $4''.0$, respectively.

In order to transform our observational sensitivities (Figure 6a) to astrophysical parameters, we substitute physical separations in AU in place of angular separations and apply the statistical relation between physical separation and semi-major axis for a sample of binaries with random inclinations and eccentricities, $\langle a \rangle = 1.26 \langle \rho \rangle$ (Fischer & Marcy 1992), obtaining Figure 7. The large plus signs in Figure 7 indicate the 90% detection limits for semi-major axes ranging from 0 to 40 AU, binned in 2 AU increments. We assume a flat contrast curve for sensitivities beyond 40 AU. Because of the large factor in distance covered by this volume-limited search, the 90% detection limits in physical separation are effectively established by the most distant stars in the sample. It is possible to boost sensitivity at closer physical separations by establishing a closer distance horizon for the search, at the expense of overall sample size. We examined the effect of using a closer distance horizon for calculating sensitivity limits, and came to the conclusion that it is more important to maintain a robust sample, especially because more sensitive but much smaller studies have

⁵GJ 169.1AB is an M4.0V/white dwarf binary. Although the brighter M4.0V component is generally considered to be the primary component, the current situation does not reflect the components' masses or spectral types at the time of stellar formation and main sequence evolution, when the current white dwarf was much more massive and luminous than the M dwarf. We therefore do not consider GJ 169.1AB to be a system with an M dwarf primary.

already been done (e.g., Close et al. 2003). We emphasize that Table 2 contains all data necessary for different statistical formulations, and is available in machine readable format in the online version of this paper.

We also considered the effect that the small field of view of *NIC2* ($19''.5 \times 19''.5$) has on sample completeness at large physical separations. Figure 8 is a histogram displaying the number of all M dwarfs, including resolved system secondaries, sampled within 10 pc ($N=141$) as a function of outer search radius, binned in 10 AU increments. While all M dwarfs were probed to semi-major axes as close as 5 AU⁶, only the farthest 12 targets were probed at semi-major axes greater than 120 AU. In order to retain the statistical significance of our sample, we consider only physical separations corresponding to mean semi-major axes between 5 and 70 AU (100% to 79.4% complete), and divide the number of companions found in the bins from 40 to 70 AU by that bin’s completeness fraction.

5.4.2. The M Dwarf Multiplicity Fraction

Table 5 lists companions to M dwarfs in our sample within our completeness range of 5 to 70 AU that were re-detected in our search or are new companions discovered during this search and published in G04. Combining these known binaries to the null detections and sensitivity limits we present in Figures 6–8, we now present formal multiplicity fractions for three distinct combinations of companion types and ranges in semi-major axes. These results are summarized in Table 6. In each case, the 1σ confidence intervals were calculated using the binomial distribution approach outlined by Burgasser et al. (2003). This approach is preferable to traditional Poisson statistics whenever the probability distribution is non-Gaussian. In each of our three different scenarios discussed below the multiplicity fraction is low enough that even with the sample of 126 systems, the probability distribution is not symmetric about the central peak value because proximity to the limiting case of a multiplicity fraction of zero causes a sharper drop-off towards the lower limit of the probability distribution (Figure 9). Given a multiplicity fraction ϵ_m , the probability distribution of finding n binaries in a sample of N systems is governed by

$$P(n) = \frac{N!}{n!(N-n)!} \epsilon_m^n (1 - \epsilon_m)^{N-n}.$$

⁶As noted in Table 2, GJ 15A, LHS 224AB, GJ 623AB, and GJ 644ABD are M dwarfs for which core saturation prevented the establishment of a sensitivity limit at $0''.2$. A single M dwarf system, GJ 747AB, saturated out to $0''.4$. All of these cases correspond to statistically corrected semi-major axes smaller than 5 AU.

This relationship can be inverted to solve for the probability distribution of a given multiplicity fraction given the observational results N and n , yielding

$$P'(\epsilon_m) = (N + 1)P(n),$$

which can then be integrated numerically to find the lower and upper limits of ϵ_m corresponding to 68% (1σ for a Gaussian distribution) of the area under the probability distribution curve, as shown by the shaded areas in Figure 9.

The M Dwarf Multiplicity Fraction for M0V to M9V Companions at Separations of 5 to 70 AU

At an inner search radius of 5 AU, our search is 90% sensitive to $M_{F180M} \lesssim 11.2$, corresponding to early L spectral types (Figure 7a). Eleven of the 12 known companions listed in Table 5 are M dwarfs meeting this sensitivity criterion. Five of these companions lie between 40 and 70 AU, where the completeness of the search is reduced due to the limited field of view. Placing these five systems into the separation bins shown in Figure 8 yields 2 systems in the 40-50 AU bin, 2 systems in the 50-60 AU bin, and one additional system in the 60-70 AU bin. Dividing these numbers by the fractional completeness of these bins (0.957, 0.879, and 0.794) and summing the results yields 5.62. We then transform the multiplicity obtained at 90% confidence level to a true volume limited multiplicity fraction by dividing 11.62 (the sum of 5.62 and the remaining companions from 5-40 AU)

by 0.9, obtaining 12.91. Rounding this number up to 13, we see that we would likely have recovered 2 additional real companions with separations ranging from 5 to 70 AU. Applying the binomial distribution, we conclude that the multiplicity fraction for M dwarf companions orbiting M dwarf primaries at semi-major axes from 5 to 70 AU is $\epsilon_m = 10.3_{-2.1}^{+3.4}\%$ (Figure 9a).

The M Dwarf Multiplicity Fraction for L0 to L9 Companions at Separations of 5 to 70 AU

Although our search did not detect any L dwarf companions within 10 pc and in the separation regime of 5 to 70 AU,⁷ it is possible to assign a multiplicity fraction based on completeness arguments. Figure 7a shows that at 5 AU, the detection rate for L dwarfs is only $\sim 50\%$. It is not possible to obtain a truly volume limited multiplicity fraction in this separation range. We therefore constrain the sample to include only the 51 systems for which

⁷GJ 1001 B and C are beyond 10 pc (Henry et al. 2006).

the detection of an L9 companion at 5 AU is possible. Applying the binomial distribution, we obtain a multiplicity fraction of $\epsilon_m = 0.0_{-0.0}^{+3.5}\%$ (Figure 9b). An alternative approach is to maintain the volume limited nature of the sample by increasing the inner limit of the separation range. From Figure 7a, the inner radius at which $>90\%$ of the systems were probed is 12 AU. We therefore calculate a volume limited multiplicity fraction for L0 to L9 companions to M dwarfs of $\epsilon_m = 0.0_{-0.0}^{+1.4}\%$ valid at separations ranging from 12 to 70 AU.

The M Dwarf Multiplicity Fraction for L0 to T9 Companions from 10 to 70 AU

Our sensitivity to T dwarfs at close separations is diminished due to their intrinsic faintness. We therefore restrict the inner search radius to 10 AU, where the search was 90% sensitive to L dwarfs and $\sim 50\%$ sensitive to late T dwarfs. At separations beyond 12 AU, Figure 7b indicates considerable scatter in the 90% sensitivity limits. Based on the trend on Figure 7b, we adopt a 90% sensitivity limit of $M_{F110W} = 17.5$, corresponding to spectral type $\sim T9$. One T6 dwarf, the class prototype GJ 229B, was detected at an inferred semi-major axis of 55.3 AU. Following the same approach we used for the L dwarfs, we calculate the multiplicity fraction for a sub sample as well as for the volume limited sample. There were 43 systems for which a late T dwarf detection at 10 AU was possible. This sub-sample yields a multiplicity fraction of $\epsilon_m = 2.3_{-0.7}^{+5.0}\%$. The complete sample is sensitive to late T dwarfs at separations ≥ 14 AU. We therefore calculate a volume limited multiplicity fraction of $\epsilon_m = 0.8_{-0.2}^{+1.8}\%$ valid at separations ranging from 14 to 70 AU.

6. Discussion

6.1. Sensitivity to Companion Masses

Estimating masses for field brown dwarfs is a difficult problem. Whereas the masses of main sequence stars can be estimated from mass-luminosity relations (Henry & McCarthy 1993; Henry et al. 1999; Delfosse et al. 2000), brown dwarfs are constantly cooling, and therefore have a mass-luminosity-age relation. Such a relation has not yet been established empirically. Currently, the best way of estimating brown dwarf masses is by correlating spectral types to effective temperatures, and then checking the effective temperature against evolutionary model predictions, assuming a certain age for the brown dwarf in question. This approach is heavily model dependent, and the end result of such calculation can at best serve as a guideline for the mass range for a particular object. With this caveat in mind, we now apply this approach to the limiting spectral types we report in Table 6.

Assuming a mean age of 3 Gyr for the nearby L dwarf field population (Seifahrt et al. 2010), the effective temperatures for brown dwarfs of spectral types L3, L5, L8, T5, and T7 are estimated to be 2000K, 1750K, 1500K, 1200K, and 900K, respectively (Golimowski et al. 2004a; Cushing et al. 2008). Adopting the evolutionary models of Chabrier et al. (2000), we estimate approximate masses of $0.073 M_{\odot}$, $0.070 M_{\odot}$, $0.057 M_{\odot}$, $0.052 M_{\odot}$, and $0.040 M_{\odot}$ for spectral types L3, L5, L8, T5, and T7 (Table 6). The last number has considerable uncertainty due to the steeper decline in effective temperatures for subtypes later than \sim T5 and the need to extrapolate the Chabrier models at low temperatures. We therefore adopt $0.040M_{\odot}$ at 3 Gyr as a guideline for the minimum mass detectable by our search. We note that the scatter in age in the nearby field population is likely to cause a large dispersion in the masses of detectable objects. Unless there are further data indicative of the age of an individual brown dwarf, the mean value we adopt here should be used with extreme caution.

6.2. A Current Map of the Brown Dwarf Desert

The idea of the brown dwarf desert continues to evolve. The term was originally used to describe the fact that radial velocity surveys of solar analogs detect an abundance of extra-solar planets but rarely detect brown dwarfs, even though a brown dwarf’s higher mass makes its detection easier. In their seminal work, Marcy & Butler (2000) found that $<1\%$ of main sequence Sun-like stars harbor brown dwarfs. Several other studies have since then obtained similar results for different ranges in separation, primary mass, and system age. Oppenheimer et al. (2001) conducted the first successful search for brown dwarf companions, discovering the T dwarf prototype GJ 229B. Their infrared coronagraphic search of stars within 8 pc detected a single substellar object, from which they cautiously imply a stellar/substellar multiplicity fraction of $\sim 1\%$. McCarthy & Zuckerman (2004) used Keck coronagraphy to search 102 nearby field GKM stars at separations from 75 to 1200 AU. They found one brown dwarf companion, and report a binary fraction of $1\pm 1\%$ ⁸. We note that their result agrees well within statistical uncertainties to our results (Table 6), suggesting a wide desert with no significant change in the substellar companion fraction from 10 to 1200 AU. Luhman et al. (2005) used *HST*’s Wide Field Planetary Camera 2 (*WFPC2*) to survey 150 members of the young cluster IC 348 (~ 2 Myr) at separations of 120–1600 AU. Of these stars, 85 were in the mass range $0.08\text{--}0.5 M_{\odot}$, approximately corresponding to the mass range for main sequence M dwarfs (Henry & McCarthy 1993). They found one possible substellar companion to a low mass star, but note that it is not possible to ascertain

⁸Using the binomial distribution treatment we adopt in this paper, 1 detection out of 102 observations is equivalent to a multiplicity fraction of $1_{-0.2}^{+3}\%$.

companionship due to the wide separation of this system (~ 1400 AU). Based on this finding, Luhman et al. derive an upper limit of 4% for the substellar companion fraction of low mass stars. This result is again in very good agreement with our results, suggesting that there is little evolution in the multiplicity fraction of low mass stars after the first few million years, and again suggesting no significant change in the substellar companion fraction beyond 10 AU. Regarding single objects, Luhman et al. find that 14 out of 150 objects are likely substellar based on evolutionary models (Chabrier et al. 2000). They note that the fact that they detect ten times more isolated stars than isolated brown dwarfs in IC 348 indicates that the brown dwarf desert may not be limited to the formation of companions, but may also extend to the formation of single objects. Metchev & Hillenbrand (2009) used adaptive optics on Keck and Palomar to survey 266 Sun-like (F5–K5) stars, and infer a brown dwarf companion frequency of $3.2^{+3.1}_{-2.7}\%$ ⁹ for separations of 28 to 1590 AU. Finally, direct imaging searches for planetary companions would be capable of detecting brighter brown dwarfs. Masciadri et al. (2005) used *VLT/NACO* to search 30 young (< 200 Myr) GKM stars and found no brown dwarf or planetary companions at separations larger than 36 AU. In a similar fashion, Biller et al. (2007) used *VLT* and *MMT* to search 45 young GKM field stars at separations of 20–40 AU, and also found no brown dwarfs. Due to smaller sample sizes, the last two studies do not add significant constraints to the brown dwarf desert, but their null detections are certainly in agreement with constraints set by the larger studies.

The sum of these studies, along with the results we present in this paper, indicate a consistent image of a brown dwarf desert that is mostly invariant with respect to the mass of the primary star, and which is valid for a wide range of separations ranging from 5 AU to 1600 AU. Whether the search is sensitive to substellar companions to Sun-like stars at intermediate to large separations (Metchev & Hillenbrand 2009), substellar companions to low mass stars at intermediate separations (our results), or a mixture of young stars with masses ranging from solar down to the M dwarf regime (Masciadri et al. 2005; Biller et al. 2007) the detection rate is always consistent with a stellar-substellar binary fraction on the order of a few percent.

6.3. Is the Desert Real?

The multiplicity fraction of Sun-like stars is $\sim 50\%$ (Duquennoy & Mayor 1991; Raghavan et al. 2010). The multiplicity rate for stellar companions to M dwarfs at all separations is $\sim 30\%$ (Henry & McCarthy 1990; Henry 1991; Fischer & Marcy 1992). Based on our results (Table

⁹ 2σ limits.

6) and the companion searches we discuss in §6.2, it is clear that stellar companions outnumber brown dwarf companions by a factor $\gtrsim 10$. Does this paucity of brown dwarfs, however, constitute a “real desert”? A few studies (e.g., Metchev & Hillenbrand 2009; Grether & Lineweaver 2006) have suggested that the dearth of brown dwarf companions is a natural consequence of a well behaved, Salpeter-like (Salpeter 1955) universal Companion Mass Function (CMF) that tends to lower multiplicities at lower mass ratios, and that a real brown dwarf desert would only exist if the observed number of brown dwarf companions is significantly lower than what a universal CMF would predict. In particular, Grether & Lineweaver note that the overlap of the planetary CMF and the stellar CMF reaches a minimum at $\sim 0.03 M_{\odot}$, causing the observed paucity of brown dwarf companions. In our search, we test the hypothesis of a universal CMF by focusing primarily on low mass stars. As shown in Table 5, the twelve M dwarf binaries we detected between 5 and 70 AU have primary masses ranging from ~ 0.6 to $\sim 0.1 M_{\odot}$. Figure 10 is a plot of the masses of the primary and the secondary components of this sample. Figure 10 shows that the mass ratios of low mass binaries tend to increase (i.e. approach equal mass components) as masses approach the hydrogen burning limit, thus excluding the formation of brown dwarf secondaries. Our completeness analysis demonstrates that this trend is not an observational selection effect. Indeed, detecting companions with higher contrasts is easier for intrinsically fainter primary stars, so the selection effect works against the trend noted in Figure 10. Reconciling our observations with the idea of a universal CMF would require this function to be rather restricted in the sense that it would not be a function of mass ratio, or would only be valid for Sun-like stars. For any reasonably broad definition, we conclude that deviations from a universal CMF do exist in the brown dwarf regime. The brown dwarf desert is therefore a reality whether one defines it in terms of total numbers or in terms of a deviation from a trend. We advocate that the concept of a universal CMF is probably not a useful representation of Nature.

6.4. More Evidence for A Discontinuity at the Hydrogen Burning Limit?

VLM binaries have a strong tendency towards high (i.e. unity) mass ratios (e.g. Burgasser et al. 2007). The effect has been demonstrated to be an intrinsic characteristic of VLM stars and brown dwarfs through Bayesian analysis (Allen 2007). Our results (Figure 10) show that mass ratios tend to increase as stellar masses approach the hydrogen burning limit, with the strong onset of nearly equal mass duplicity happening somewhere between 0.2 and $0.1 M_{\odot}$. Other studies have also suggested that the basic population properties of Initial Mass Function (IMF), CMF, and the binary separation distribution all appear to change significantly at a mass of $\sim 0.1 M_{\odot}$, slightly above the hydrogen burning limit. Close et al. (2003) conducted

an adaptive optics search of 39 VLM objects with spectral types ranging from M8.0V to L0.5, and found a mass distribution similar to the one shown in Figure 10 (see their Table 3). They also probed smaller separations than our formal limit of 5 AU, and found that whereas higher mass stars have a separation distribution peaked at 30 AU (Duquennoy & Mayor 1991), VLM binaries have a separation distribution peaked at 4 AU. Also, Bayesian analysis of several studies (Allen 2007) demonstrates that VLM and brown dwarf binaries with separations > 20 AU are extremely rare. We note that Close et al. probed significantly smaller separations than we did, but did not establish formal detection limits. Kraus et al. (2005) conducted a search for VLM binaries in the Upper Scorpius OB association, and also found results consistent with a discontinuity in the separation distribution at a mass of $0.1M_{\odot}$.

In an analysis of data from several open cluster studies, Thies & Kroupa (2007) demonstrate that the observed mass distribution is incompatible with the existence of an IMF that is monotonic about the hydrogen burning limit. They note that because stellar formation and stellar ignition are in principle unrelated processes governed by different areas of physics, there is no reason to expect that the IMF discontinuity would be caused by the onset of hydrogen burning. They therefore allow for an arbitrary overlap of the stellar and brown dwarf components of the IMF, thus allowing for a smooth turnover. In light of our companion mass distribution for low mass stars (Figure 10), new developments in the hydrodynamical simulations of star cluster formation (Bate 2009, 2011), and new observations of young stellar clusters (Kraus et al. 2008, 2011; Evans et al. 2012), we re-examine the nature of the IMF discontinuity at masses close to the hydrogen burning limit.

The details of the mass function for older field objects close to the hydrogen burning limit are difficult to quantify. The difficulty is mostly due to the lack of a robust volume limited census of L and T dwarfs based on trigonometric parallaxes or reliable distance estimates (errors $< 20\%$). For the M dwarfs, the situation is more clear. Our recent results from the *RECONS* 10 pc census indicate a *minimum* M dwarf space density of $0.057pc^{-3}$ (Henry et al. 2006)¹⁰. Cruz et al. (2007) find a space density of $4.9 \times 10^{-3}pc^{-3}$ for M dwarfs later than M7V and a lower limit of $3.8 \times 10^{-3}pc^{-3}$ for L dwarfs. Assuming that field age ($\sim 1-5$ Gyr) brown dwarfs with masses slightly below the hydrogen burning limit are predominately mid to late L dwarfs (§6.1, Table 7), and that stars of spectral type M7V or later have masses $\lesssim 0.1 M_{\odot}$ (Henry et al. 1999; Delfosse et al. 2000), the ratio of objects with masses above and below $0.1 M_{\odot}$ is 6.9. The shape of the M dwarf distribution in the *RECONS* 10 pc

¹⁰ $0.059pc^{-3}$ for epoch 2012.0. See www.recons.org for the latest numbers and analysis. Comparison of the 10 pc sample with the 5 pc sample indicates that the 10 pc M dwarf sample is $\sim 70\%$ complete. We note, however, that an analysis of the *RECONS* sensitivity limits indicates that the assumption of a representative M dwarf sample within 5 pc may be significantly biased by statistics of small numbers.

census corresponds broadly to the distribution of our *NICMOS* sample, (Figure 1), with the drop-off happening at around spectral type M6V, corresponding to $\sim 0.1 M_{\odot}$. Even if the actual density for L dwarfs is a few times greater than the lower limit of Cruz et al. (2007), there is still a significant difference in the number of stars versus brown dwarfs.

Could the onset of core hydrogen fusion cause the discontinuity in the IMF and the CMF via a radiative feedback mechanism? We caution that our understanding of stellar formation processes in this mass range is rather limited from a theoretical as well as an empirical basis, so any explanation is tentative at best. We speculate that if the onset of core hydrogen burning at ages from 3–5 Myr (Chabrier & Baraffe 1997) has a significant role in hindering accretion, the star formation process would produce a discontinuity at masses $\gtrsim 0.075 M_{\odot}$. Although it has been generally accepted that protostars acquire the bulk of their mass during the first 1 Myr, observations show that a sizable fraction of substellar objects continue to accrete for a much longer time. Jayawardhana et al. (2003) find that 40%–60% of brown dwarfs in young star forming regions with ages up to ~ 10 Myr show infrared excesses consistent with accretion. There is also observational evidence that at least some high mass brown dwarfs undergo phases of strong accretion comparable to the T Tauri phases of more massive stars (Bouy et al. 2008; Comerón et al. 2010). For the highest mass proto-brown dwarfs, late accretion may be enough to ignite hydrogen fusion, or to otherwise significantly change the manner in which the young object interacts with its environment. More observations and theoretical work are needed to confirm or discard this hypothesis, in particular with regards to testable predictions of accretion rates. Even if late accretion brings the total mass of a proto-brown dwarf above the hydrogen burning limit, we lack a clear understanding of how the onset of core hydrogen fusion would hinder accretion. At ages of a few Myr, the vast majority of an object’s luminosity comes from the release of internal gravitational energy, so the onset of hydrogen burning would have a negligible effect on overall luminosity (Chabrier & Baraffe 1997). We note, however, that hydrodynamical cluster collapse simulations (Bate 2009) are in good agreement with the stellar IMF and stellar CMF, but overproduce the number of brown dwarfs unless radiative feedback is incorporated into the model (Bate 2011). The last model produces a cluster of stars and brown dwarfs whose statistical properties are very similar to those of observed young clusters, suggesting that radiative feedback is indeed an important mechanism in brown dwarf formation. If the discontinuity in the CMF and the IMF at $0.1 M_{\odot}$ stands up to further observational scrutiny, a strong convergence of theoretical models and observational evidence will be needed to prove this or other hypotheses.

7. Conclusions

We conducted a large, volume-limited, high resolution search for substellar companions around nearby stars, with a particular emphasis on M dwarf systems. By evaluating the completeness and sensitivity of the search, we have established the multiplicity fractions for M dwarfs listed in Table 6. We find a multiplicity fraction of $0.0^{+3.5}_{-0.0}\%$ for L companions to M dwarfs with semi-major axis ranging from 5 to 70 AU. Including T dwarfs down to spectral type T9 and restricting the inner search radius to 10 AU yields a multiplicity fraction of $2.3^{+5.0}_{-0.7}\%$. These rates are far less than M dwarf pairs, for which we found a multiplicity fraction of $10.3^{+3.4}_{-2.1}\%$ for separations of 5 to 70 AU. Based on these results, we summarize the substellar multiplicity fraction for M dwarfs as being on the order of a few percent or less. As discussed in §6.2, several other multiplicity studies have reached essentially the same conclusion regardless of primary mass, the separations probed, or the sample’s age estimate. The emerging picture is that of a pervasive “brown dwarf desert”, hinting to origins that are largely independent of a binary’s formation mechanism. By specifically focusing on low mass primaries, our study has weakened the case for mass ratio dependence in the formation of substellar companions. We add ours to a list of several studies that indicate that the companion mass function is truncated at a mass $\sim 0.1 M_{\odot}$, slightly above the hydrogen burning mass limit (§6.4, Figure 10). While the primary focus of this work is characterizing the companion population, we also note in §6.4 that the results we obtain for the stellar/substellar multiplicity fraction are consistent with estimates for the population density of isolated brown dwarfs. The similarity suggests that mechanisms causing the observed paucity of brown dwarfs, both as companions and as isolated objects, may be intrinsic to the brown dwarf formation process. Recent results from hydrodynamic cluster collapse simulations as well as evidence for T Tauri like accretion at ages of a few Myr make radiative feedback from recently ignited very low mass stars a good candidate mechanism for truncating the IMF and the CMF at masses slightly above the hydrogen burning mass limit.

The authors thank Russel White, Deepak Raghavan, and Adam Burgasser for useful conversations. We thank our anonymous referee for many insightful comments that greatly improved the paper. This work is based on observations made with the NASA/ESA *Hubble Space Telescope*, obtained at the Space Telescope Science Institute, which is operated by the Association of Universities for Research in Astronomy, Inc., under NASA contract NAS 5-26555. These observations are associated with *HST* programs 7420, 7894, and 9485. Support for these observations was provided by NASA through grants HST-GO-07420, HST-GO-07894, and HST-GO-09485 from the Space Telescope Science Institute (STScI).

REFERENCES

- Allard, F., Hauschildt, P. H., Baraffe, I., & Chabrier, G. 1996, *ApJ*, 465, L123
- Allen, P. R. 2007, *ApJ*, 668, 492
- Allen, P. R., Koerner, D. W., McElwain, M. W., Cruz, K. L., & Reid, I. N. 2007, *AJ*, 133, 971
- Allen, P. R., & Reid, I. N. 2008, *AJ*, 135, 2024
- Bate, M. R. 2009, *MNRAS*, 392, 590
- . 2011, *MNRAS*, 417, 2036
- Biller, B. A., et al. 2007, *ApJS*, 173, 143
- Bochanski, J. J., Hawley, S. L., Covey, K. R., West, A. A., Reid, I. N., Golimowski, D. A., & Ivezić, Ž. 2010, *AJ*, 139, 2679
- Bouy, H., et al. 2008, *A&A*, 486, 877
- Burgasser, A. J., Kirkpatrick, J. D., Reid, I. N., Brown, M. E., Miskey, C. L., & Gizis, J. E. 2003, *ApJ*, 586, 512
- Burgasser, A. J., Reid, I. N., Siegler, N., Close, L., Allen, P., Lowrance, P., & Gizis, J. 2007, *Protostars and Planets V*, 427
- Chabrier, G., & Baraffe, I. 1997, *A&A*, 327, 1039
- Chabrier, G., Baraffe, I., Allard, F., & Hauschildt, P. 2000, *ApJ*, 542, 464
- Close, L. M., Siegler, N., Freed, M., & Biller, B. 2003, *ApJ*, 587, 407
- Comerón, F., Testi, L., & Natta, A. 2010, *A&A*, 522, A47
- Cruz, K. L., et al. 2007, *AJ*, 133, 439
- Cushing, M. C., et al. 2008, *ApJ*, 678, 1372
- Dahn, C. C., et al. 2002, *AJ*, 124, 1170
- Delfosse, X., Forveille, T., Ségransan, D., Beuzit, J.-L., Udry, S., Perrier, C., & Mayor, M. 2000, *A&A*, 364, 217
- Duquennoy, A., & Mayor, M. 1991, *A&A*, 248, 485

- Evans, T. M., et al. 2012, *ApJ*, 744, 120
- Fischer, D. A., & Marcy, G. W. 1992, *ApJ*, 396, 178
- Forveille, T., et al. 2004, *A&A*, 427, L1
- Geballe, T. R., et al. 2002, *ApJ*, 564, 466
- Gizis, J. E., Reid, I. N., Knapp, G. R., Liebert, J., Kirkpatrick, J. D., Koerner, D. W., & Burgasser, A. J. 2003, *AJ*, 125, 3302
- Golimowski, D. A., et al. 2004a, *AJ*, 127, 3516
- . 2004b, *AJ*, 128, 1733
- Grether, D., & Lineweaver, C. H. 2006, *ApJ*, 640, 1051
- Henry, T. J. 1991, PhD thesis, Arizona Univ., Tucson.
- Henry, T. J., Franz, O. G., Wasserman, L. H., Benedict, G. F., Shelus, P. J., Ianna, P. A., Kirkpatrick, J. D., & McCarthy, Jr., D. W. 1999, *ApJ*, 512, 864
- Henry, T. J., Jao, W.-C., Subasavage, J. P., Beaulieu, T. D., Ianna, P. A., Costa, E., & Méndez, R. A. 2006, *AJ*, 132, 2360
- Henry, T. J., & McCarthy, Jr., D. W. 1990, *ApJ*, 350, 334
- . 1993, *AJ*, 106, 773
- Jayawardhana, R., Ardila, D. R., Stelzer, B., & Haisch, Jr., K. E. 2003, *AJ*, 126, 1515
- Knapp, G. R., et al. 2004, *AJ*, 127, 3553
- Kraus, A. L., Ireland, M. J., Martinache, F., & Hillenbrand, L. A. 2011, *ApJ*, 731, 8
- Kraus, A. L., Ireland, M. J., Martinache, F., & Lloyd, J. P. 2008, *ApJ*, 679, 762
- Kraus, A. L., White, R. J., & Hillenbrand, L. A. 2005, *ApJ*, 633, 452
- Krist, J. E., Golimowski, D. A., Schroeder, D. J., & Henry, T. J. 1998, *PASP*, 110, 1046
- Krist, J. E., & Hook, R. N. 1997, in *The 1997 HST Calibration Workshop with a New Generation of Instruments*, ed. S. Casertano, R. Jedrzejewski, T. Keyes, & M. Stevens, 192–+
- Lowrance, P. J., et al. 2005, *AJ*, 130, 1845

- Luhman, K. L., McLeod, K. K., & Goldenson, N. 2005, *ApJ*, 623, 1141
- Marcy, G. W., & Butler, R. P. 2000, *PASP*, 112, 137
- Masciadri, E., Mundt, R., Henning, T., Alvarez, C., & Barrado y Navascués, D. 2005, *ApJ*, 625, 1004
- McCarthy, C., & Zuckerman, B. 2004, *AJ*, 127, 2871
- Metchev, S. A., & Hillenbrand, L. A. 2009, *ApJS*, 181, 62
- Nakajima, T., Oppenheimer, B. R., Kulkarni, S. R., Golimowski, D. A., Matthews, K., & Durrance, S. T. 1995, *Nature*, 378, 463
- Oppenheimer, B. R., Golimowski, D. A., Kulkarni, S. R., Matthews, K., Nakajima, T., Creech-Eakman, M., & Durrance, S. T. 2001, *AJ*, 121, 2189
- Raghavan, D., et al. 2010, *ApJS*, 190, 1
- Reid, I. N., Cruz, K. L., Burgasser, A. J., & Liu, M. C. 2008, *AJ*, 135, 580
- Reid, I. N., & Gizis, J. E. 1997, *AJ*, 113, 2246
- Rosenthal, E. D., Gurwell, M. A., & Ho, P. T. P. 1996, *Nature*, 384, 243
- Salpeter, E. E. 1955, *ApJ*, 121, 161
- Seifahrt, A., Reiners, A., Almaghrbi, K. A. M., & Basri, G. 2010, *A&A*, 512, A37
- Skrutskie, M. F., et al. 2006, *AJ*, 131, 1163
- Thies, I., & Kroupa, P. 2007, *ApJ*, 671, 767
- Tinney, C. G., Burgasser, A. J., Kirkpatrick, J. D., & McElwain, M. W. 2005, *AJ*, 130, 2326
- York, D. G., et al. 2000, *AJ*, 120, 1579
- Viana, A., Wiklind, T., et al. 2009, *NICMOS Instrument Handbook*, Version 11.0, (Baltimore: STScI).
- Thatte, D. and Dahlen, T. et al. 2009, *NICMOS Data Handbook*, version 8.0, (Baltimore, STScI)

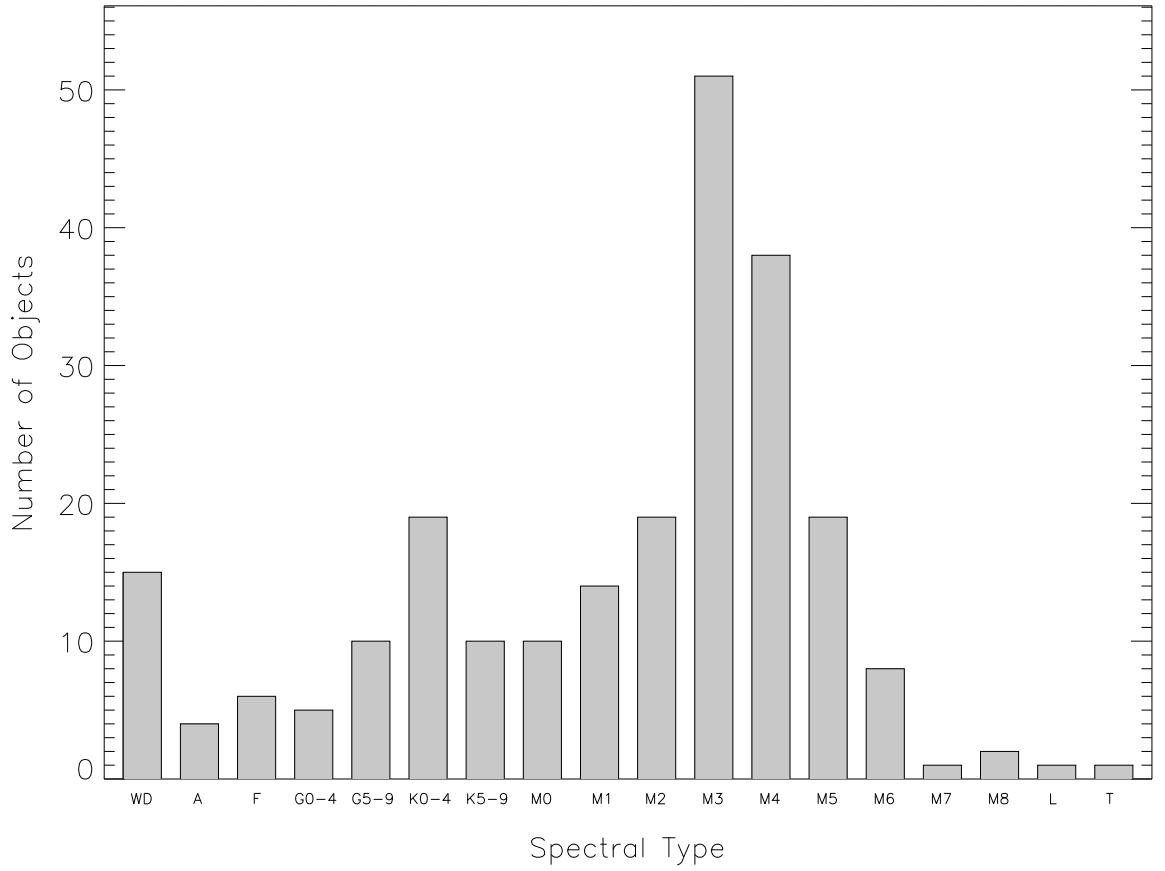


Fig. 1.— Spectral type distribution of the 239 targets within 10 pc in the search. The sample constitutes 69% of the *RECONS* 10 pc sample (epoch 2012.0). 63% of the targets are M dwarfs, which is in close agreement with the M dwarf distribution of the 10 pc sample, 69% (epoch 2012.0).

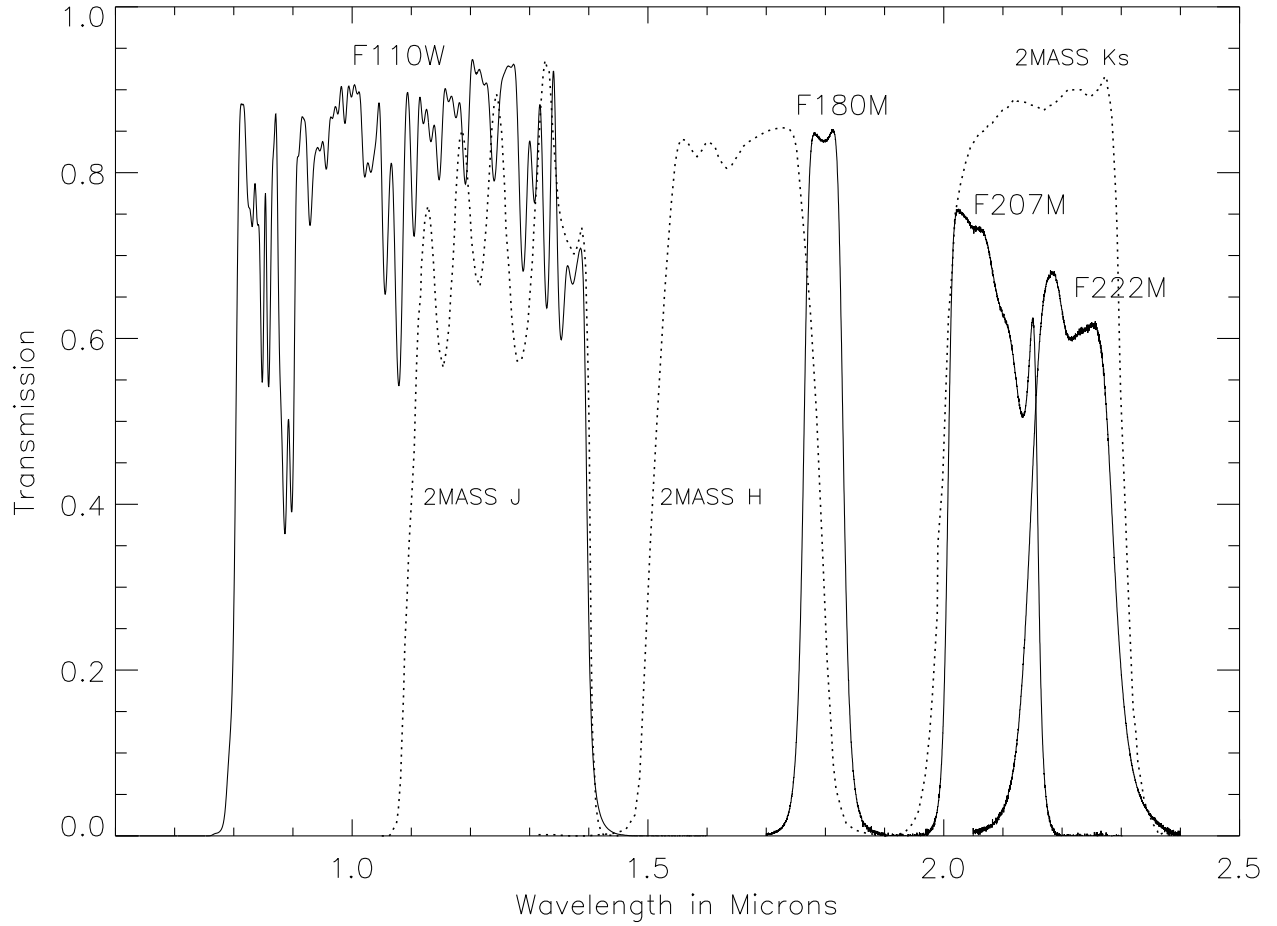


Fig. 2.— Transmission curves for the four *NICMOS* filters used in the survey. The *2MASS* filters are plotted with dotted lines for comparison. Although no individual *NICMOS* filter is a close match to a ground based equivalent, together they cover nearly the same wavelength range of ground based near infrared color systems.

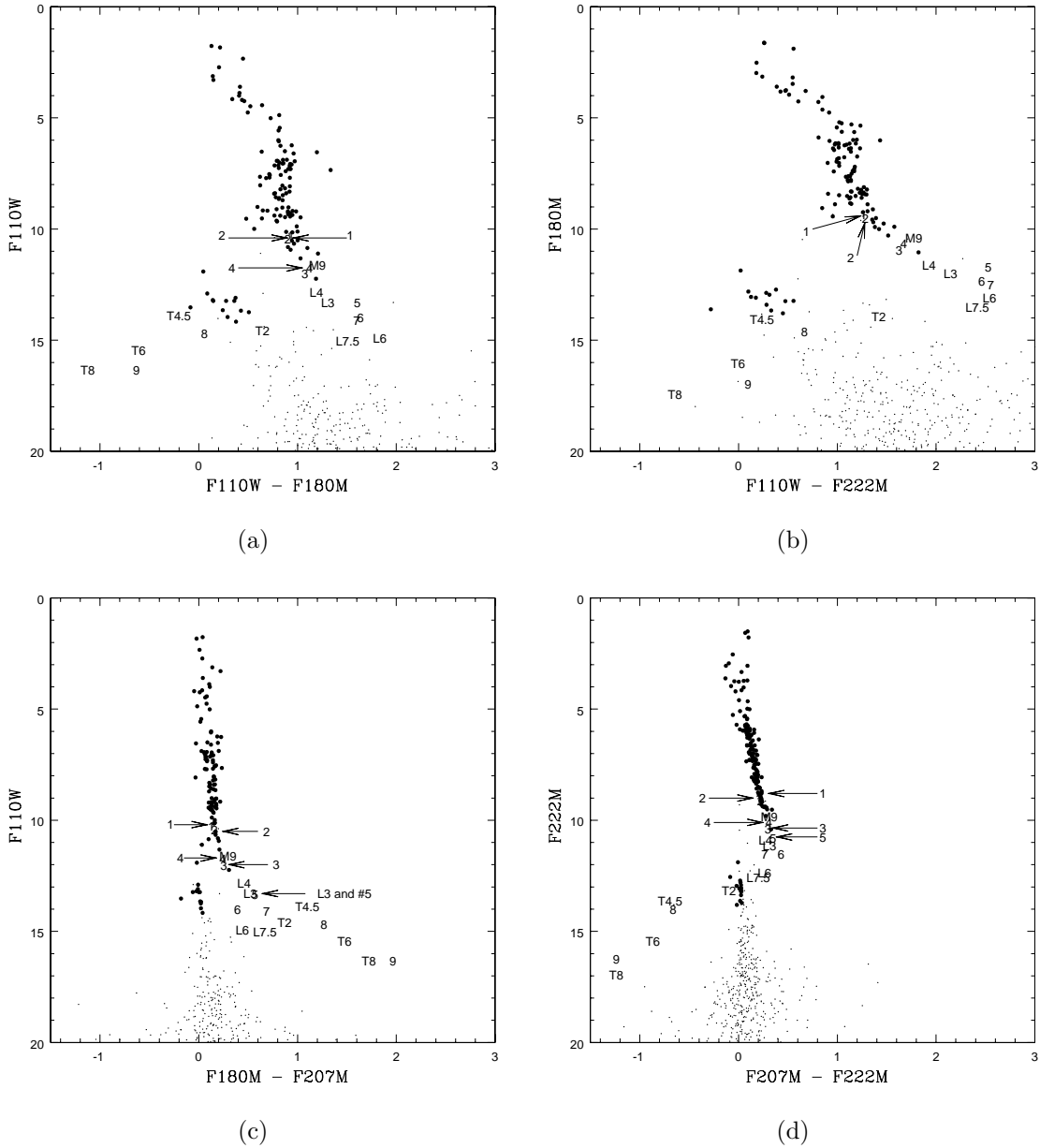
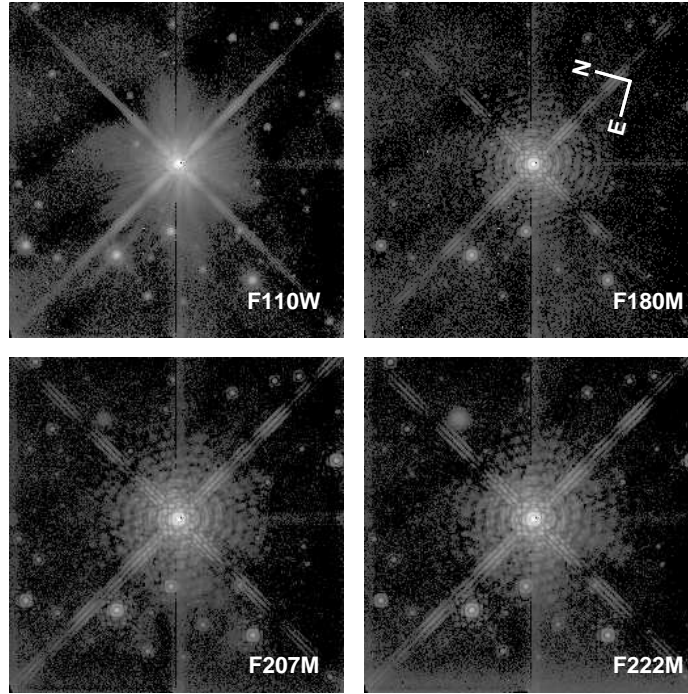
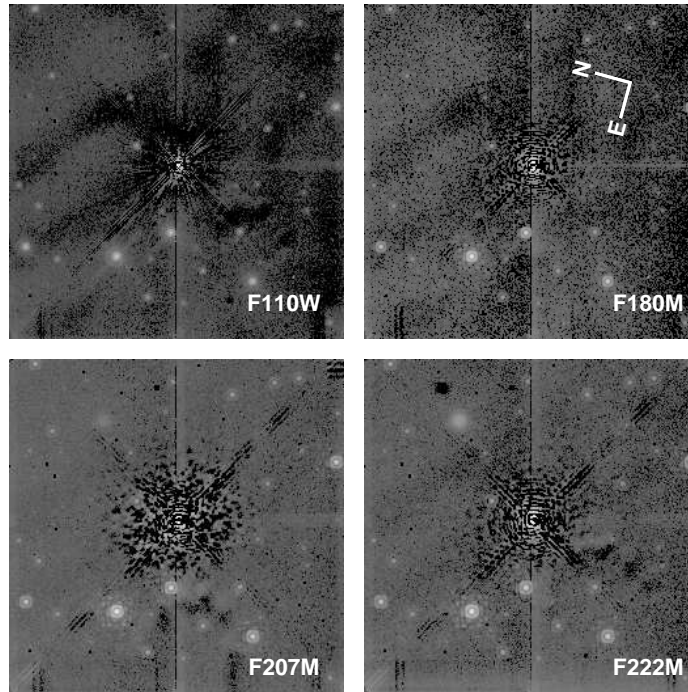


Fig. 3.— Selected color-magnitude diagrams designed to detect substellar companions. The large dots are the primary targets of the search, including 13 white dwarfs. The small dots are background objects. Synthetic photometry of L and T dwarfs, as well as one M9 dwarf, is plotted using a label for spectral type, with the precise dot position at the center of the label. In these diagrams, all objects within the field of view of a primary target are plotted assuming a common parallax (i.e. companionship). Only if the assumption is correct would the object fit in the stellar or substellar sequence. The benchmark objects discussed in §5.1.1 are labeled as follows: (1) GJ 1245A, (2) GJ 1245B, (3) G 239-25B, (4) GJ 1245C, (5) GJ 1001BC (combined), (6) GJ 1001B, (7) GJ 1001C, (8) 2MA 0559-1404, and (9) GJ 229B. Panels (a) and (b) illustrate the drastic color shift around spectral type L6 caused by the onset of CH_4 absorption. The reduced effect of interstellar reddening on background objects displayed in panels (c) and (d), as well as the large shift from red to blue for substellar objects, make these bands particularly useful for methane imaging.

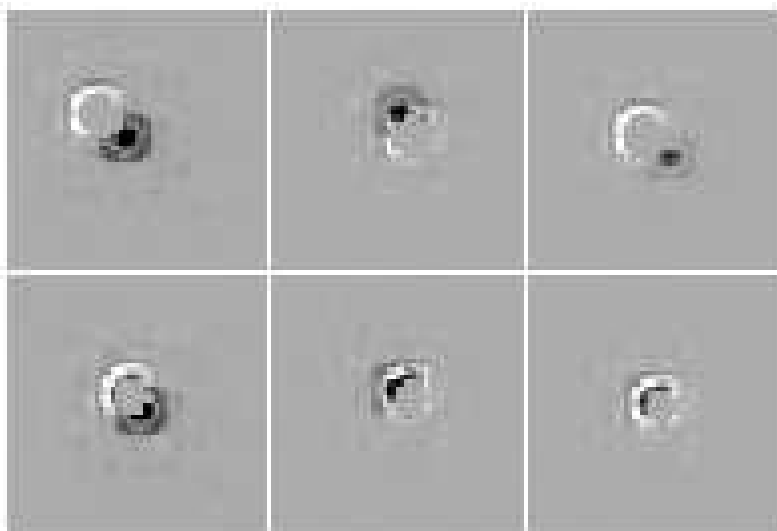


(a)

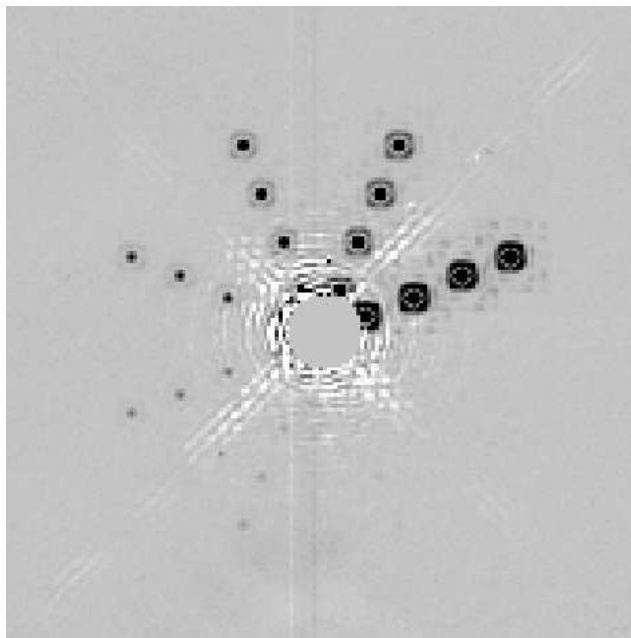


(b)

Fig. 4.— Survey images for LHS 288 (M5.5V) using logarithmic scaling. The frames illustrate typical survey images both before (a) and after (b) PSF subtraction. The ghost-like coronagraphic artifact is visible in the upper left hand corner, particularly in the $F222M$ images. The highly structured PSF of the primary target dominates the field before PSF subtraction.

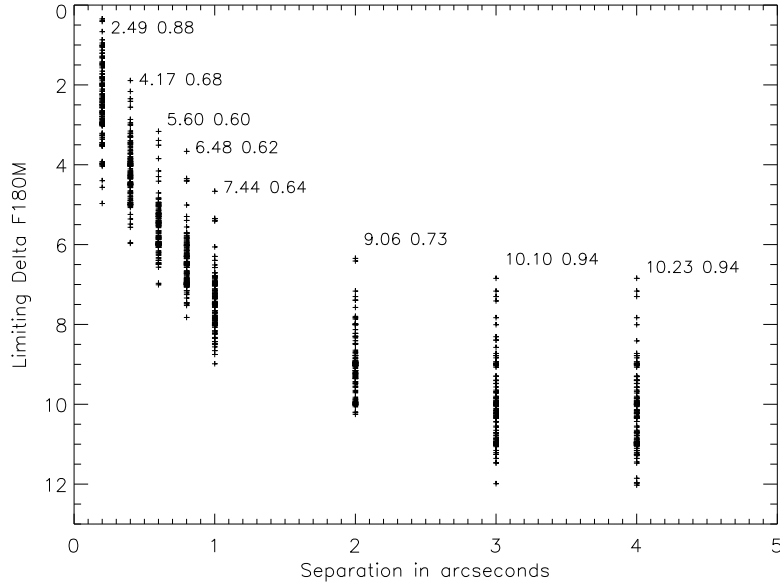


(a)

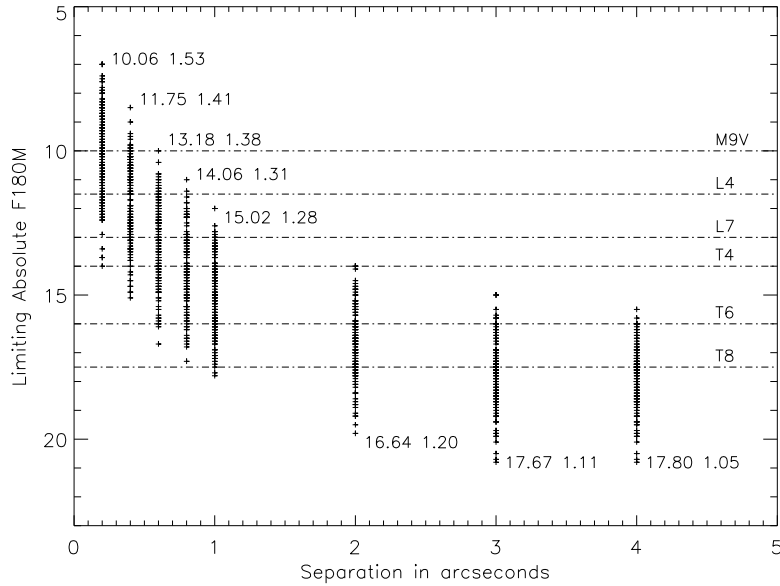


(b)

Fig. 5.— Examples of sensitivity simulations around GJ 213 (M4.0V, $F180M=6.68$). (a) To test sub-arcsecond separations, a mosaic of PSF insertions with several separations and magnitudes is created. In this figure the rows represent separations of $0''.2$ (bottom), and $0''.4$ (top). The columns represent apparent $F180M$ magnitudes of 9, 10, and 11 from left to right. The artificial companions are visible at all three magnitudes for $0''.4$ but only at the brightest magnitude for $0''.2$. (b) PSF insertions are laid out in a radial pattern to test the sensitivity at separations of $1''.0$ and greater. Apparent $F180M$ magnitudes range from 12 to 19 in increments of 1, with the rays for 18 and 19 not detectable in this case. Separations are $1''.0$, $2''.0$, $3''.0$, and $4''.0$. In both simulations the residuals of the PSF subtraction are set to zero at a radius interior to the artificial companions to facilitate detection. A thorough inspection requires using surface and contour plots.

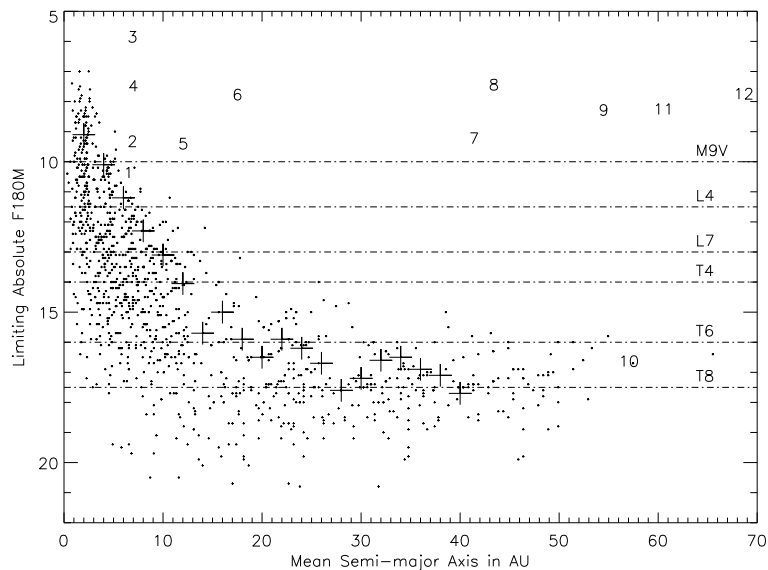


(a)

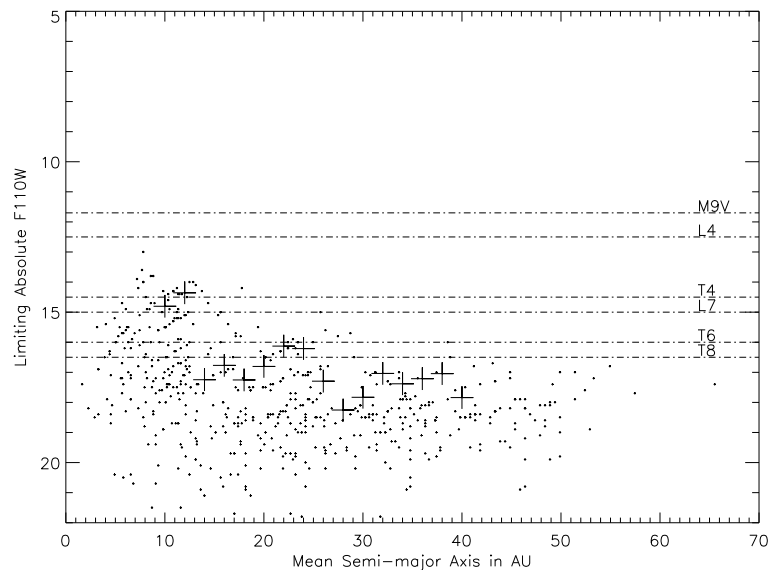


(b)

Fig. 6.— Search sensitivities for the eight angular separations tested by PSF insertion simulations. In both panels, the two numbers next to each cluster of points are the mean and standard deviation for that separation, respectively. (a) The ability to detect a companion is primarily determined by the angular separation and the components’ Δm . This instrumental representation has a lower standard deviation, but does not probe fundamental astrophysical parameters. (b) Transforming Δm into absolute magnitudes yields a range of possible companion types detectable at each angular separation. The absolute $F180M$ magnitude for select spectral subtypes is taken from the synthetic photometry displayed in Figure 3b.



(a)



(b)

Fig. 7.— (a) Search sensitivity displayed as a function of absolute $F180M$ magnitude and mean semi-major axis, assuming $\langle a \rangle = 1.26 \langle \rho \rangle$ (Fischer & Marcy 1992). Each dot represents the sensitivity derived from a PSF insertion around an M dwarf (Table 2). The range of limiting absolute magnitudes is significantly wider at close separations because all targets were probed at close physical separations, whereas only targets close to our distance limit of 10 pc could be probed at wide physical separations given *NIC2*'s small field of view. Contrast is also more strongly dependent on overall brightness at close angular separations. The large plusses represent the absolute magnitude limits where 90% of companions can be detected at a given physical separation. The numbers indicate the positions of the companions listed in Table 5: (1) GJ 84B, (2) GJ 65B, (3) GJ 661B, (4) GJ 257B, (5) GJ 1116B, (6) GJ 860B, (7) GJ 1245B, (8) GJ 896B, (9) GJ 1230B, (10) GJ 229B, (11) GJ 618B, and (12) LP 771-95B. The large blank space in the center and right-hand-side of the diagram is a clear representation of the “brown dwarf desert”. (b) Same as (a), but using absolute $F110W$, and omitting separations $\leq 1''$. While the sensitivity to T dwarfs is increased in (b), the sensitivity to L dwarfs is decreased and close separations cannot be probed. See §5.3 for discussion.

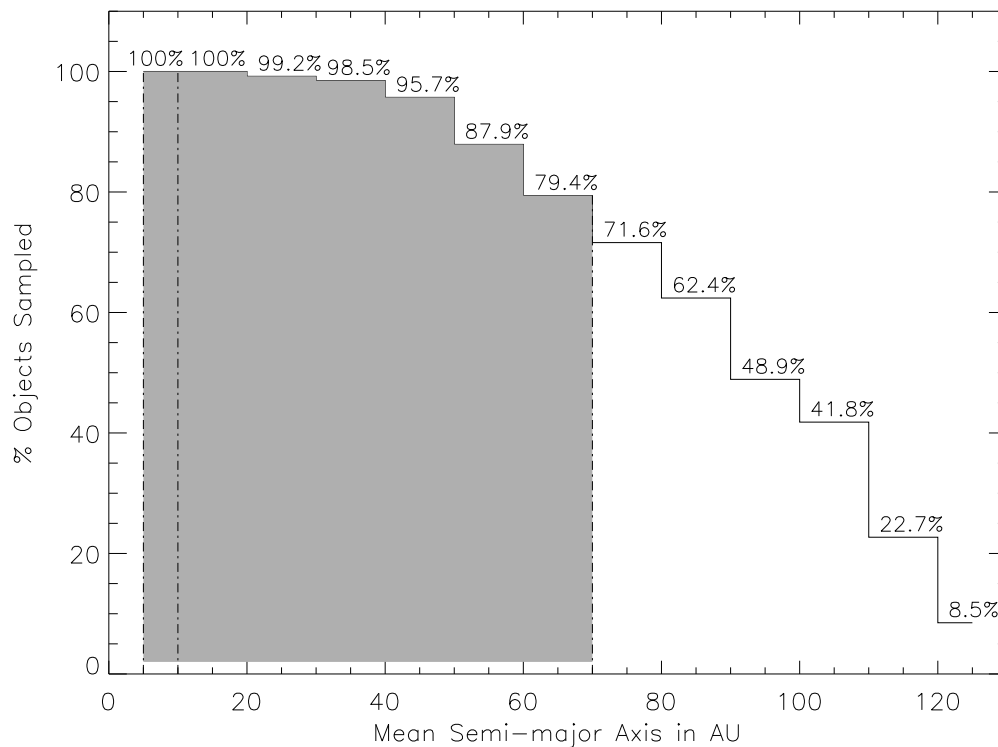


Fig. 8.— Statistical semi-major axis distribution for companion search around all 141 M dwarf components within 10 pc. The shaded area indicates the separation ranges we consider when calculating the multiplicity fraction, with the dashed lines indicating the inner radius limits for M and L dwarfs (5 AU), and for the T dwarfs (10 AU) and the outer radius for both (70 AU). Search completeness diminishes with increasing separation because *NIC2*'s field of view limits our search radius to $\sim 9''$.

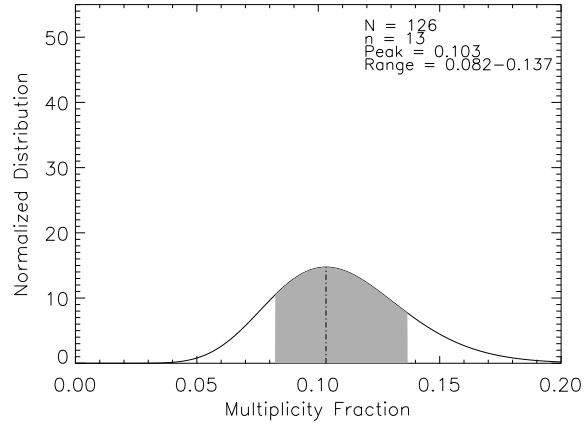
Table 1. Sample Tallies

Sub-sample	Tally
<i>HST</i> Visits	217
Total Resolved Targets ^a	233
Total Unresolved Targets ^b	22
Total Star Systems ^c	201
Resolved Targets within 10 pc ^a	218
Unresolved Targets within 10 pc ^b	21
Star Systems within 10 pc ^c	188
Resolved M Dwarfs within 10 pc ^a	141
Systems with M Dwarf Primary within 10 pc ^c	126
Resolved Targets beyond 10 pc ^a	15
Unresolved Targets beyond 10 pc ^b	1
Star Systems beyond 10 pc ^c	13

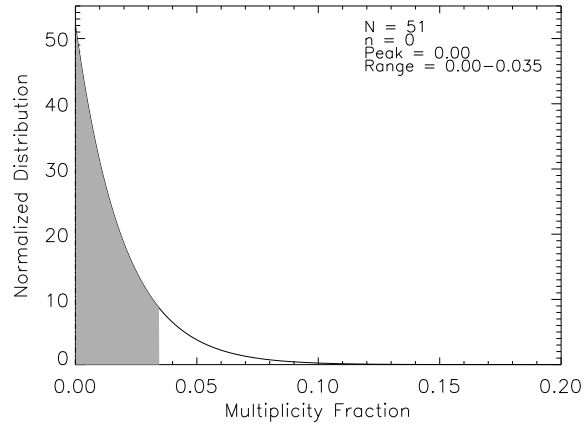
^aEach PSF not known to be a blend of more than one star or brown dwarf and that is not a background source is counted as one “resolved target”.

^bEach PSF known to be the blend of two or more stars or brown dwarfs in the same system is counted as one “unresolved target”.

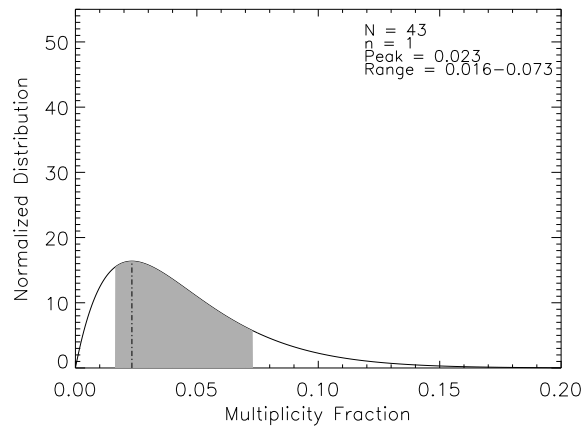
^cDenotes known physical association at any physical separation, including systems comprising multiple fields of view.



(a)



(b)



(c)

Fig. 9.— Probability density distributions for select multiplicity fractions listed in Table 6, calculated using the binomial distribution. The shaded areas correspond to 68% of the area under the curve, equivalent to the 1σ confidence range. The individual plots correspond to: (a) M dwarf companions, (b) L dwarf companions, (c) L and T dwarf companions.

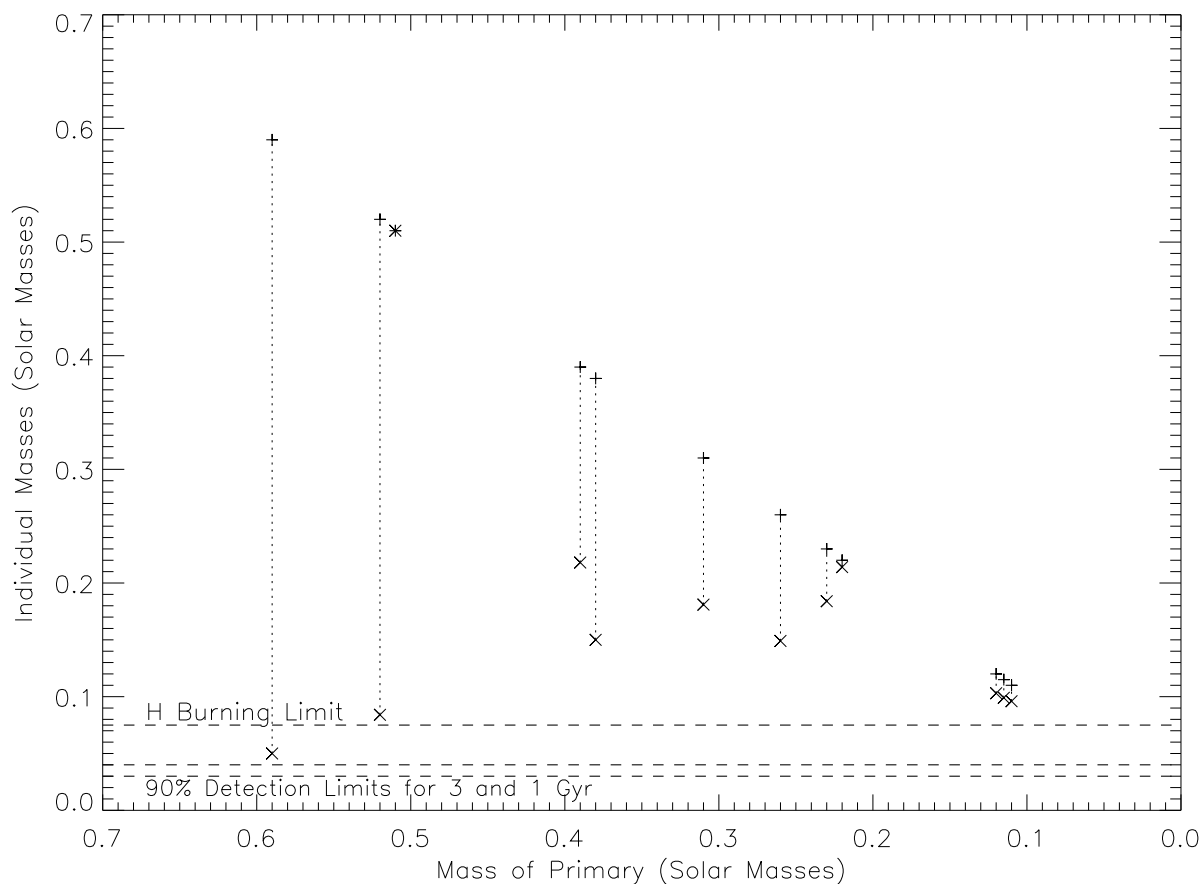


Fig. 10.— Mass distribution for the binaries in Table 5. The horizontal dashed lines denote the hydrogen burning limit ($0.075 M_{\odot}$) and the 90% detection limits for this search assuming brown dwarf ages of 1 Gyr and 3 Gyr (Table 7). As the masses of the primary components approach the hydrogen burning limit, the mass ratios tend to unity, thus implying that brown dwarfs rarely form as secondaries. See §6.3–6.4 for discussion. From left to right, the binaries are ordered as they appear in Table 5.

Table 2. Sensitivity to Companions

Name	Resolved PSFs in FOV ¹	Spectral Type	Distance (pc)	Epoch	App. Mag. (<i>F180M</i>)	Absolute <i>F180M</i> Magnitude Limit								Notes
						0''2	0''4	0''6	0''8	1''0	2''0	3''0	4''0	
GJ 915	...	DA5	8.1	2003 Jun 3	12.53	11.9	12.4	14.4	14.4	14.9	15.4	15.4	15.4	a
GJ 1001A	A	M3.0V	13.0	1998 Aug 3	7.97	8.4	11.9	13.4	13.9	14.4	16.4	16.4	16.4	b,g
GJ 1	...	M1.5V	4.3	1998 Jan 10	4.64	8.0	11.0	12.5	13.0	14.5	16.5	17.5	18.5	...
GJ 1002	...	M5.0V	4.6	2002 Oct 27	7.79	12.4	13.4	14.9	15.9	16.4	18.4	19.4	19.4	...
GJ 1005AB	AB	M3.5VJ	5.9	2002 Oct 3	6.71	10.1	12.1	13.1	14.1	15.1	17.1	18.1	18.1	b,d,f
GJ 15A	A	M1.5V	3.5	2003 Jun 26	4.48	...	10.7	12.2	12.2	13.2	15.2	16.2	16.2	b,d,i
GJ 15B	B	M3.5V	3.5	1998 Aug 19	6.20	12.4	12.4	14.4	15.4	15.4	17.4	18.4	18.4	b
GJ 17	...	F9.5V	8.5	1997 Aug 29	2.81	...	8.1	9.1	10.1	10.6	13.1	14.1	15.1	i
GJ 19	...	G0.0V	7.4	1998 Feb 2	1.25	8.4	9.4	11.4	12.9	13.4	i
GJ 2012	...	DQ9	9.0	1997 Dec 31	13.58	15.8	16.8	16.8	16.8	17.8	17.8	17.8	17.8	a
GJ 33	...	K2.5V	7.4	1998 Oct 8	3.58	...	8.7	10.2	11.2	11.2	13.2	15.2	15.2	i
GJ 34A	A	G3V	5.9	2002 Sep 10	2.09	6.7	6.2	6.7	9.2	10.2	10.2	b,d,i
GJ 34B	A/B	K7.0V	5.9	1998 Aug 27	4.03	...	10.2	11.2	11.7	12.7	15.2	16.2	16.2	b
GJ 35	...	DZ7	4.3	1997 Oct 1	11.56	16.4	17.4	18.4	18.4	19.4	19.9	19.9	19.9	...
GJ 48	...	M2.5V	8.2	1998 Oct 16	5.70	10.1	10.6	11.6	13.1	13.6	15.6	17.1	17.1	...
GJ 53AB	A/B	K1.0VI	7.5	2002 Oct 11	3.60	...	7.6	8.6	10.6	11.6	13.6	14.6	15.6	b ₁ ,d,f,h,i
GJ 54AB	AB	M3.0VJ	7.8	1998 Nov 9	5.80	9.3	10.3	11.8	12.3	13.3	15.3	17.3	17.3	b,c
GJ 54.1	...	M4.0V	3.7	2002 Sep 17	6.73	12.1	13.1	15.1	16.1	17.1	19.1	20.1	20.1	...
GJ 65A	A/B	M5.5V	2.6	2002 Nov 8	6.40	11.9	12.9	14.9	15.4	15.9	16.9	17.9	18.9	b,h
GJ 65B	A/B	M6.0V	2.6	2002 Nov 8	6.58	11.9	12.9	14.9	14.9	15.9	16.9	17.9	18.9	b,h
GJ 66A	A	K2.0V	7.6	2002 Sep 22	6.68	...	7.6	9.1	9.6	10.1	11.6	13.6	13.6	b,d,i
GJ 66B	A/B	K2.0V	7.6	2002 Nov 16	6.74	...	8.1	8.6	9.6	10.6	12.6	13.6	13.6	b,d,e,i
GJ 68	...	K1.0V	7.5	1997 Oct 20	3.32	...	7.9	9.9	10.9	11.9	13.9	14.9	15.9	...
LHS 145	...	DA7	9.7	2002 Oct 18	12.66	13.7	14.7	16.7	17.2	17.7	18.7	18.7	18.7	a
GJ 71	...	G8.5V	3.6	1997 Aug 14	1.59	10.8	11.3	11.8	13.8	15.8	16.8	...
GJ 75	...	G9.0V	10.0	1998 Aug 28	3.81	...	8.8	10.3	10.8	11.3	13.8	14.8	14.8	i
LHS 1302	...	M4.5V	9.9	2002 Oct 10	8.76	11.3	12.8	14.3	14.8	15.8	17.8	18.8	18.8	...
GJ 83.1	...	M4.0V	4.4	2002 Nov 24	6.90	11.7	12.7	14.7	15.2	16.2	17.7	18.7	18.7	...
LHS 1326	...	M5.5V	8.9	1997 Sep 17	9.26	12.0	14.5	15.5	16.0	16.5	17.5	18.5	18.5	e
GJ 84AB	A/B	M2.5VJ	9.1	2002 Oct 2	5.75	9.4	10.9	11.4	12.9	13.4	14.9	16.9	16.9	b,f
LHS 1339	...	M2.5V	9.2	2002 Oct 1	7.78	10.9	11.9	12.9	13.9	14.9	16.9	16.9	16.9	...
LHS 1375	...	M5.5V	8.5	1997 Oct 28	9.34	13.7	14.7	16.7	16.7	17.7	17.7	17.7	17.7	...
GJ 105AC	A/C	K3.0V	7.1	1998 Jan 9	9.19	0.9	13.9	15.9	16.9	17.9	18.9	20.9	21.9	b,f,i
APMPM J0237-5928	...	M4.5V	9.6	2002 Jul 24	8.68	11.8	12.8	13.8	14.8	15.8	17.8	17.8	17.8	...

Table 2—Continued

Name	Resolved PSFs in FOV ¹	Spectral Type	Distance (pc)	Epoch	App. Mag. (<i>F180M</i>)	Absolute <i>F180M</i> Magnitude Limit								Notes
						0 ^h 2	0 ^h 4	0 ^h 6	0 ^h 8	1 ^h 0	2 ^h 0	3 ^h 0	4 ^h 0	
LP 771-95A	A/B/C	M2.5V	6.9	2003 Jun 18	6.76	11.1	12.6	13.1	14.6	15.6	16.6	17.6	18.6	b
LP 771-95B	A/B/C	M3.5VJ	6.9	2003 Jun 18	7.12	10.9	11.9	13.9	14.9	15.9	16.9	17.9	...	b,e,h
LP 771-95C	A/B/C	M3.5VJ	6.9	2003 Jun 18	7.68	12.0	12.5	14.0	14.5	16.5	17.5	18.5	19.5	b,e,h
GJ 1057	...	M4.5V	8.5	1998 Jan 7	8.17	11.5	12.5	14.5	15.0	16.0	17.5	17.5	17.5	...
GJ 137	...	G5V	9.1	2002 Oct 5	3.04	...	7.2	8.2	9.2	10.2	12.2	13.2	14.2	d,i
GJ 139	...	G8.0V	6.0	1997 Oct 20	2.51	...	9.6	10.1	11.1	11.6	12.6	14.6	15.6	i
GJ 144	...	K2.0V	3.2	2002 Oct 18	1.88	10.5	11.0	11.0	12.5	14.5	14.5	c,d,i
GJ 1061	...	M5.0V	3.6	2002 Jul 29	6.97	12.1	13.1	14.6	15.1	16.1	18.1	19.1	19.1	...
GJ 1068	...	M4.0V	6.9	2002 Jul 22	8.21	11.8	13.8	14.8	14.8	15.8	17.8	17.8	17.8	d,i
GJ 166A	A	K0.5V	4.9	2003 Feb 23	2.59	10.0	10.5	11.5	13.0	14.5	14.5	b,d,i
GJ 166B	B	DA4	4.9	2003 Apr 1	9.99	12.0	13.5	14.0	14.5	15.5	17.5	17.5	...	a,b,d,e
GJ 169.1A	A	M4.0V	5.5	2002 Oct 8	5.91	10.2	11.7	13.2	14.2	14.7	16.7	18.2	18.2	b
GJ 169.1B	A/B	DC5	5.5	2002 Aug 3	11.80	15.1	16.1	17.1	18.1	19.1	21.1	21.1	21.1	a,b,e
LHS 194	...	DQ7	9.5	1998 Apr 13	12.85	14.0	15.0	16.5	17.0	18.0	18.5	20.0	20.0	a
GJ 176	...	M2.0V	9.0	2003 Feb 17	5.68	9.9	10.9	12.4	13.4	13.9	15.9	16.9	16.9	...
GJ 178	...	F6V	8.0	1998 Feb 20	2.05	...	7.5	9.5	10.0	10.5	12.5	13.5	14.5	i
LHS 1731	...	M3.0V	9.2	2002 Sep 21	7.22	10.2	11.2	12.7	13.7	14.2	15.2	17.2	17.2	...
GJ 191	...	M2.0VI	3.9	1997 Oct 18	5.12	9.2	11.2	12.2	13.2	14.2	16.2	18.2	18.2	...
GJ 203	...	M3.0V	9.7	1997 Dec 22	7.80	8.9	11.9	13.9	14.4	15.9	16.9	18.9	18.9	...
GJ 213	...	M4.0V	5.8	1997 Aug 9	6.68	10.8	12.3	13.8	14.8	15.8	17.8	18.8	18.8	...
GJ 216B	B	K2.5V	8.9	2002 Oct 13	4.16	...	8.7	9.2	10.2	10.7	13.2	14.2	14.2	b,d,i
GJ 222AB	AB	G0.0VJ	8.6	1998 Aug 15	2.91	6.2	7.7	9.2	10.7	11.2	13.2	14.2	15.2	b,c,i
GJ 223.2	...	DZ9	6.4	1998 May 4	12.84	14.8	17.8	19.3	19.8	20.8	20.8	20.8	20.8	a
2MA 0559-1404	...	T4.5	10.2	2003 Jan 23	14.60	15.6	17.6	19.1	19.6	20.6	20.6	20.6	20.6	a,g
G 99-49	...	M3.5V	5.2	2003 Jan 8	6.33	10.7	12.2	12.7	14.2	15.2	16.7	17.7	18.7	...
LHS 1805	...	M3.5V	7.5	2003 Mar 8	6.91	10.5	12.5	13.5	14.0	15.0	16.5	18.5	18.5	...
LHS 1809	...	M5.0V	9.2	1998 Feb 12	8.73	11.9	12.4	14.9	15.9	16.4	17.9	18.9	18.9	...
GJ 226	...	M2.5V	9.3	1998 Feb 15	6.26	9.4	10.4	11.9	12.9	13.4	15.4	17.4	17.4	...
GJ 229A	A/B	M1.5V	5.7	1997 Aug 15	4.19	8.4	9.4	10.4	11.4	12.9	15.4	17.4	17.4	b
GJ 232	...	M4.0V	8.3	1997 Dec 20	8.19	11.6	13.6	14.6	15.6	16.1	18.6	18.6	18.6	...
L 032-009(A)	A	M2.5V	9.0	2003 May 7	5.72	9.4	10.4	11.9	12.9	13.4	15.9	16.9	16.9	b
L 032-008(B)	B	M3.0V	9.0	2002 Sep 23	6.49	9.7	10.7	12.7	13.7	14.2	16.7	17.7	17.7	b
GJ 244AB	A/B	A1.0V	2.6	2003 Mar 27	-1.39	6.0	8.5	9.5	9.5	b,d,f,i
GJ 250B	B	M2.0V	8.7	1998 Mar 24	5.89	8.2	10.2	12.2	13.2	14.2	16.2	17.2	17.2	b

Table 2—Continued

Name	Resolved PSFs in FOV ¹	Spectral Type	Distance (pc)	Epoch	App. Mag. (<i>F180M</i>)	Absolute <i>F180M</i> Magnitude Limit								Notes
						0'2	0'4	0'6	0'8	1'0	2'0	3'0	4'0	
GJ 257A	A/B	M3.0V	8.0	1998 Oct 30	7.15	10.5	10.5	12.5	13.5	14.5	15.5	17.5	17.5	b,h
GJ 257B	A/B	M3.0V	8.0	1998 Oct 30	7.18	10.5	11.5	12.5	13.5	14.5	15.5	17.5	17.5	b,h
GJ 1093	...	M5.0V	7.7	1997 Aug 29	8.56	12.1	13.1	15.1	16.1	16.6	18.1	18.1	18.1	...
LHS 224AB	A/B	M4.5VJ	9.2	2003 Mar 13	8.71	...	12.9	15.4	15.9	17.9	18.9	19.9	19.9	b,c
GJ 280A	A	F5.0IV-V	3.5	2003 Jan 11	-0.67	6.8	8.3	10.3	11.3	a,b,d,f,i
GJ 283A	A	DZQ6	9.1	2003 Mar 20	12.64	13.8	15.8	16.8	17.8	18.8	19.8	19.8	19.8	a,b
GJ 283B	B	M6.5V	9.1	2003 Mar 25	9.74	12.9	14.9	15.4	15.9	16.9	18.9	19.9	19.9	b
GJ 1103	...	M4.5V	8.7	2002 Sep 9	8.03	12.3	13.3	14.8	14.8	15.3	17.3	18.3	18.3	...
GJ 293	...	DQ9	7.9	2002 Aug 29	12.49	15.5	16.0	17.0	18.0	19.5	21.0	21.0	21.0	a
GJ 1105	...	M4.0V	8.2	2003 Mar 10	7.14	11.1	12.1	13.1	14.1	15.1	16.6	17.6	17.6	...
GJ 2066	...	M4.0V	6.8	1998 Sep 17	5.86	9.2	10.2	11.7	13.2	13.7	14.7	16.7	16.7	...
GJ 1111	...	M6.0V	3.6	2003 Mar 2	7.68	13.4	14.9	15.9	16.4	17.4	18.4	19.9	19.9	...
GJ 318	...	DA6	8.8	2003 Jul 4	11.60	13.9	14.9	15.9	16.9	18.4	21.9	20.9	20.9	a
GJ 1116A	A/B	M5.5VJ	5.2	1998 Nov 9	7.83	10.2	12.2	14.7	15.7	16.2	18.2	19.2	19.2	b,h
GJ 1116B	...	M5.5VJ	5.2	1998 Nov 9	8.17	10.6	12.6	13.1	14.6	16.1	17.6	18.6	18.6	b,h
LHS 2090	...	M6.0V	6.3	2003 Jan 25	8.77	12.3	13.8	15.8	17.3	17.8	19.8	20.8	20.8	...
GJ 338A	A	M0.0V	6.1	2002 Nov 27	4.04	8.6	10.6	11.1	11.6	12.6	14.1	16.1	16.1	b,d,i
GJ 341	...	M0.0V	10.4	1997 Oct 15	5.73	7.6	9.6	11.6	12.6	13.1	14.6	16.6	16.6	g
GJ 357	...	M2.0V	9.0	2003 Feb 13	6.72	10.9	12.9	13.4	14.4	14.9	16.9	17.9	17.9	...
GJ 1128	...	M4.0V	6.5	1998 Nov 1	7.31	11.7	12.7	14.2	14.7	16.2	17.2	19.2	19.2	...
GJ 367	...	M2.0V	9.7	1997 Sep 17	5.99	8.5	11.0	12.0	13.0	13.5	16.0	17.0	17.0	...
GJ 370	...	K6V	11.1	1997 Aug 12	4.86	8.6	9.6	10.6	11.6	12.1	14.6	15.6	16.6	g
LHS 2206	...	M4.0V	9.2	2003 Feb 19	8.66	10.8	12.3	13.8	15.8	16.3	18.8	19.8	19.8	...
GJ 380	...	K7.0V	4.8	2003 Feb 19	3.30	6.6	8.1	9.6	11.1	12.1	14.6	15.6	15.6	d,i
GJ 388	...	M2.5V	4.8	1998 Mar 26	4.81	8.9	11.4	12.4	13.4	13.9	16.4	17.4	17.4	...
GJ 393	...	M2.0V	7.1	2003 Jun 16	5.46	9.7	11.2	12.7	13.2	13.7	16.2	17.2	17.2	...
LHS 288	...	M5.5V	4.7	1997 Jul 31	6.14	9.2	11.7	13.7	14.2	15.2	16.7	17.7	17.7	...
LHS 292	...	M6.5V	4.5	2004 Jun 2	8.26	11.2	13.2	14.7	15.7	16.7	19.2	20.7	20.7	a,d
GJ 1138AB	A/B	M4.5VJ	9.7	2003 May 10	8.04	10.1	12.1	14.1	15.1	15.1	16.1	17.1	17.1	b,c,d
GJ 402	...	M4.0V	6.8	1998 Mar 15	6.67	10.5	12.0	13.5	14.0	15.0	16.5	17.5	17.5	...
GJ 406	...	M5.5V	2.3	2003 Feb 27	6.41	14.0	14.5	16.0	16.5	17.5	19.5	20.5	20.5	...
GJ 408	...	M2.5V	6.7	2003 Feb 6	5.60	10.0	11.0	12.5	13.5	14.5	15.5	17.5	17.5	...
GJ 411	...	M2.0V	2.5	2003 Jun 22	3.72	10.0	11.0	13.0	13.5	14.5	16.0	17.0	18.0	d,i
GJ 412A	A	M1.0V	4.8	2003 Jun 14	5.00	10.6	11.1	12.6	13.6	14.6	15.6	17.6	17.6	b,d,i

Table 2—Continued

Name	Resolved PSFs in FOV ¹	Spectral Type	Distance (pc)	Epoch	App. Mag. (<i>F180M</i>)	Absolute <i>F180M</i> Magnitude Limit								Notes
						0'2	0'4	0'6	0'8	1'0	2'0	3'0	4'0	
GJ 412B	B	M5.5V	4.8	2003 May 5	8.23	11.8	14.3	15.8	16.8	17.3	18.8	19.8	19.8	b
GJ 432A	A	K0.0V	9.5	2003 Mar 2	4.14	...	9.1	10.1	10.6	12.1	13.1	14.1	14.1	b,d,i
GJ 432B	B	DC	9.5	2004 Jun 29	13.67	15.1	15.6	17.1	17.1	17.6	17.6	17.6	17.6	a,b,h
GJ 433	...	M2.0V	8.9	2003 Feb 3	5.76	8.5	10.5	12.0	13.0	14.0	15.0	16.0	16.0	...
GJ 434	...	G8.0V	9.6	1997 Dec 13	3.64	4.6	7.6	10.1	10.6	11.6	13.1	14.1	15.1	...
GJ 438	...	M1.0V	10.9	2002 Sep 3	6.58	8.8	10.3	11.8	12.3	13.3	14.8	15.8	15.8	d,g,i
GJ 440	...	DQ6	4.6	1997 Jul 29	11.20	16.7	17.7	18.7	18.7	18.7	19.7	19.7	19.7	e
GJ 442A	A	G2.0V	9.2	1998 Aug 16	3.30	5.7	8.2	9.2	10.2	11.7	12.7	14.2	15.2	b
GJ 442B	B	M4.0V:	9.2	2002 Aug 31	8.24	9.7	11.7	13.7	14.2	15.2	17.2	17.2	17.2	b
GJ 445	...	M3.5V	5.3	2003 Mar 28	6.24	9.9	11.9	12.9	13.9	14.9	16.4	18.4	18.4	...
GJ 447	...	M4.0V	3.3	1997 Jul 13	5.93	10.9	12.9	14.4	15.4	16.9	18.4	19.4	19.4	...
GJ 1151	...	M4.5V	8.1	1997 Jul 15	7.93	10.4	13.4	14.4	15.4	16.4	17.4	17.4	17.4	...
GJ 450	...	M1.5V	8.6	2003 Apr 2	5.74	8.8	9.8	11.3	12.3	13.3	15.3	16.3	16.3	...
GJ 451	...	K1.0VI	9.0	2003 Mar 5	4.50	7.7	9.2	10.7	11.2	12.2	14.2	15.2	15.2	d,i
GJ 1154	...	M4.5V	8.3	1998 Mar 15	7.84	9.9	12.4	13.9	15.4	16.4	17.4	18.4	18.4	...
GJ 475	...	G0.0V	8.4	1997 Aug 6	2.80	4.4	6.4	8.9	9.4	11.4	12.4	14.4	15.4	...
GJ 479	...	M2.5V	9.6	2003 Jul 3	6.30	9.1	11.1	12.1	12.1	14.1	16.1	17.1	17.1	...
LHS 337	...	M4.0V	6.3	1998 Sep 3	7.70	10.5	12.5	14.0	15.0	16.5	17.0	18.0	18.0	...
GJ 480.1	...	M3.0V	7.9	2003 Jan 7	7.68	9.5	12.5	14.0	15.0	16.0	16.5	16.5	17.5	...
GJ 486	...	M4.0V	8.3	2003 May 16	6.66	9.4	11.4	12.4	12.9	14.4	15.4	17.4	17.4	...
GJ 493.1	...	M4.5V	8.1	1997 Aug 14	7.97	11.0	13.5	14.5	15.0	16.5	17.5	17.5	17.5	...
GJ 494	...	M0.0V	11.4	1997 Aug 13	5.74	8.2	10.7	11.7	12.2	13.7	14.7	15.7	16.7	g
GJ 506	...	G7.0V	8.5	2003 Jul 1	2.97	...	7.3	8.3	9.3	10.3	12.3	13.3	14.3	d,i
GJ 518	...	DZ9	8.2	1998 Jan 3	12.81	14.9	15.4	16.9	17.4	17.4	17.9	a,e
LHS 2784	...	M3.5V	9.2	2002 Dec 5	7.29	9.2	11.2	13.2	14.2	15.7	16.7	18.2	18.2	...
GJ 551	C	M5.0V	1.3	2003 Apr 6	4.84	10.4	12.9	14.4	15.4	16.4	17.4	19.4	19.4	b,d,i
LHS 2930	...	M6.5V	9.6	1997 Oct 18	10.21	12.1	15.1	16.1	16.6	17.1	17.6	17.6	17.6	e
GJ 555	...	M4.0V	6.2	1998 Mar 20	6.19	10.5	11.5	13.0	13.5	15.0	16.0	18.0	18.0	...
GJ 559A	A	G2.0V	1.3	1998 Oct 22	-1.89	7.9	8.9	9.9	12.4	12.4	a,b,d,i
GJ 559B	B	K0V	1.3	1998 Oct 19	8.4	9.9	11.4	13.4	13.4	a,b,i
G 239-25AB	A/B	M3VJ	9.8	1998 Nov 7	6.73	9.0	11.0	12.0	13.5	14.0	16.0	17.0	17.0	b,f,g
GJ 566A	A/B	G7.0V	6.7	1998 Sep 14	2.94	8.8	10.8	12.8	13.8	14.8	14.8	b,h,i
GJ 566B	A/B	K4V	6.7	1998 Sep 14	6.8	8.8	8.8	10.3	11.8	a,b,e,h,i
TVLM 513-46546	...	M9.0V	10.5	2002 Sep 8	11.16	11.4	13.4	14.9	15.4	16.4	17.4	17.9	17.9	a,e,g

Table 2—Continued

Name	Resolved PSFs in FOV ¹	Spectral Type	Distance (pc)	Epoch	App. Mag. (<i>F180M</i>)	Absolute <i>F180M</i> Magnitude Limit								Notes
						0''2	0''4	0''6	0''8	1''0	2''0	3''0	4''0	
GJ 581	...	M3.0V	6.3	1998 May 6	6.07	9.5	11.5	13.0	14.0	15.5	17.0	18.0	18.0	...
GJ 588	...	M2.5V	5.9	1997 Sep 18	4.95	7.6	10.6	12.1	13.1	14.6	16.1	17.1	17.1	...
GJ 609	...	M3.5V	9.9	1997 Dec 31	7.62	10.5	13.0	13.5	14.5	15.0	17.0	17.5	17.5	...
GJ 618B	A/B	M4.5V	8.3	1998 Oct 14	8.83	9.9	11.4	12.4	12.9	13.9	16.4	16.4	16.4	b,e
GJ 623AB	AB	M2.5VJ	8.0	1998 Sep 11	6.16	...	10.5	11.5	13.0	13.5	15.5	16.5	16.5	b,c
GJ 625	...	M1.5V	6.5	2002 Sep 10	5.94	7.9	10.9	11.9	12.9	13.9	15.9	16.9	17.9	...
GJ 628	...	M3.5V	4.2	1997 Aug 12	5.37	9.8	10.8	12.8	14.3	14.8	16.8	17.8	17.8	...
GJ 631	...	K0.0V	9.7	1998 Jul 13	3.69	7.1	9.1	10.1	11.1	11.6	13.1	14.1	15.1	...
GJ 633	...	M2.5V	21.9	1997 Sep 6	8.33	10.3	11.3	12.8	13.3	14.8	15.3	15.3	15.3	g
GJ 638	...	K7.0V	9.8	2002 Aug 28	4.88	7.0	9.0	10.0	10.5	11.5	14.0	15.0	16.0	d
GJ 643	...	M3.0V	6.4	2002 Oct 15	7.03	11.5	12.5	14.0	15.0	16.0	18.0	19.0	19.0	...
GJ 644ABD	A/BD	M2.5VJ	6.4	1998 Oct 15	4.78	...	8.0	10.0	10.5	11.5	13.0	15.0	16.0	b,c,d
GJ 644C	C	M7.0V	6.4	2003 Jun 8	9.20	12.0	14.0	16.0	16.5	17.0	18.0	18.0	18.0	b,d
GJ 1207	...	M3.5V	8.6	1997 Sep 16	7.29	10.3	12.3	13.8	14.3	15.8	17.3	17.3	17.3	...
GJ 649	...	M0.5V	10.2	1997 Sep 23	5.69	7.9	9.9	10.9	12.9	14.4	15.9	16.9	16.9	g
LHS 3262	...	M5.0V	9.4	1997 Aug 17	8.07	10.1	13.1	14.6	15.1	16.1	17.1	17.6	17.6	...
G 203-47AB	AB	M3.5VJ	7.4	2002 Nov 8	6.76	10.1	12.1	13.1	14.1	14.6	16.6	17.6	17.6	b,c,d
GJ 661AB	A/B	M3.0VJ	6.4	2002 Aug 26	5.07	7.5	9.5	11.0	13.0	13.5	16.0	17.5	18.0	b,d,f,h
GJ 664	...	K5.0V	5.9	2002 Oct 22	10.6	11.1	12.6	14.1	15.1	15.1	d
GJ 666B	A/B	K7.0V	8.7	1998 Oct 26	4.95	8.3	9.8	11.3	12.3	13.3	15.3	16.3	16.3	b
GJ 667A	A/B	K4.0VJ	7.2	2003 Feb 1	3.23	6.7	7.7	8.7	9.7	10.7	12.7	14.7	15.7	b,d,h,i
GJ 667B	A/B	K4.0VJ	7.2	2003 Feb 1	3.23	6.7	8.7	9.7	9.7	11.7	13.7	15.7	15.7	b,d,h,i
GJ 673	...	K7.0V	7.7	1997 Oct 27	4.20	6.6	8.6	10.6	11.6	13.1	14.6	15.6	16.6	...
GJ 674	...	M2.5V	4.5	1997 Sep 7	5.02	9.7	10.7	12.7	13.7	14.7	16.7	17.7	17.7	...
GJ 678.1	...	M0.5V	9.9	2002 Aug 22	5.65	7.0	10.0	11.5	12.0	13.0	15.0	16.0	16.0	d
GJ 682	...	M4.0V	5.0	1998 Oct 30	5.79	8.5	11.5	13.5	14.0	15.0	16.5	17.5	17.5	...
GJ 687	...	M3.0V	4.5	1998 Feb 5	4.61	8.7	10.2	12.7	13.2	13.7	15.7	17.7	17.7	...
GJ 686	...	M0.5V	8.0	1997 Aug 1	5.69	8.5	10.5	12.5	14.0	14.5	15.5	16.0	16.5	...
GJ 694	...	M3.0V	9.5	1998 Jul 24	6.10	9.1	10.1	11.6	13.1	14.1	16.1	17.1	17.1	...
GJ 2130BC	...	M2.0V	14.1	1998 Sep 17	6.75	8.7	10.2	11.2	12.2	13.2	16.2	16.2	16.2	b,c,g
GJ 1221	...	DXP9	6.0	1997 Aug 15	12.48	16.1	17.1	18.1	19.1	19.1	19.1	19.1	19.1	...
GJ 699	...	M3.5V	1.8	1997 Sep 21	4.82	10.7	12.7	14.7	15.7	17.2	17.7	19.7	19.7	...
GJ 701	...	M1.0V	7.7	1997 Aug 14	5.45	8.5	10.5	12.5	13.0	14.0	14.5	15.5	15.5	...
GJ 702A	A/B	K0.0V	5.1	2002 Sep 18	1.88	8.5	9.5	10.5	12.5	14.5	14.5	b,d,i

Table 2—Continued

Name	Resolved PSFs in FOV ¹	Spectral Type	Distance (pc)	Epoch	App. Mag. (<i>F180M</i>)	Absolute <i>F180M</i> Magnitude Limit								Notes
						0''2	0''4	0''6	0''8	1''0	2''0	3''0	4''0	
GJ 702B	A/B	K5.0V	5.1	2002 Sep 18	1.88	...	6.5	8.5	10.5	12.5	13.5	14.5	14.5	b,d,e,i
GJ 1224	...	M4.0V	7.5	1997 Sep 19	7.98	11.6	12.6	14.1	14.6	16.6	17.6	18.6	18.6	...
LHS 3376	...	M4.5V	7.2	2002 Aug 20	8.26	12.2	13.7	14.2	14.7	16.2	17.2	17.7	17.7	...
GJ 713AB	AB	F7VJ	8.1	2003 Feb 28	2.37	7.5	8.5	9.5	11.5	13.5	13.5	b,c,d,i
GJ 1227	...	M4.5V	8.2	1997 Jul 30	7.93	12.4	13.4	14.4	15.4	15.9	17.4	17.4	17.4	...
GJ 721	...	A0.0V	7.7	2002 Dec 12	-0.03	4.1	5.6	8.6	9.6	9.6	a,d,i
GJ 1230AC	AC/B	M4.0VJ	8.2	2003 Jan 23	6.91	8.4	9.9	12.4	12.9	13.4	16.4	17.4	17.4	b,c,d
GJ 1230B	AC/B	M5.0V	8.2	2003 Jan 23	8.03	11.4	13.4	14.4	15.4	16.4	17.4	17.4	17.4	b,d,e
GJ 725A	A	M3.0V	3.5	1998 Jul 21	4.59	9.3	10.3	12.3	13.3	15.3	16.3	17.3	17.3	b
GJ 725B	B	M3.5V	3.5	1998 Oct 13	5.15	8.3	11.3	13.3	14.3	15.3	17.3	18.3	18.3	b
GJ 745A	A	K7.0V	8.6	1998 Aug 25	6.68	9.8	11.3	12.3	13.3	14.3	15.3	17.3	17.3	b
GJ 745B	B	M1.0V	8.6	2002 Oct 7	6.75	9.3	10.3	12.3	13.3	14.3	15.3	17.3	17.3	b,d,e
GJ 747AB	AB	M3.5VJ	8.1	2002 Dec 11	6.66	10.4	11.4	12.4	14.4	15.4	17.4	a,b,c,d
GJ 752A	A	M2.5V	5.8	1998 Nov 10	4.73	8.7	10.2	11.7	12.2	13.2	15.2	16.2	17.2	b
GJ 752B	B	M8.0V	5.8	2002 Aug 6	9.18	12.2	14.2	15.2	16.2	17.2	19.2	19.2	19.2	b
GJ 1235	...	M4.0V	9.9	1997 Aug 16	8.14	11.0	13.0	14.0	15.5	16.0	17.0	18.0	18.0	...
GJ 764	...	G9.0V	5.7	2003 Jan 1	3.04	...	8.2	9.2	10.2	11.7	13.2	14.2	15.2	i
GJ 768	...	A7.0V	5.1	1997 Oct 13	0.18	8.5	9.5	10.5	12.5	13.0	13.5	i
GJ 1245AC	A/B/C	M5.5VJ	4.5	1998 Oct 10	7.32	11.7	12.7	14.2	15.2	16.2	17.7	18.7	18.7	b,f,h
GJ 1245B	A/B/C	M6.0V	4.5	2003 Feb 14	7.67	11.2	12.7	13.7	14.7	15.7	17.7	18.7	18.7	b
GJ 780	...	G8.0IV	6.1	1997 Aug 25	1.92	...	7.1	8.6	10.1	11.1	13.1	14.1	14.1	i
GJ 783A	A/B	K2.5V	6.0	2003 Mar 21	3.00	...	8.1	9.1	9.6	10.6	13.1	14.1	14.1	b,d,i
GJ 783B	A/B	M2.5V	6.0	2003 Mar 21	...	9.1	11.1	12.1	13.1	14.1	16.1	17.1	17.1	b,e
GJ 784	...	M0.0V	6.2	1997 Oct 14	4.39	7.0	10.0	11.5	12.0	13.0	15.0	16.0	16.0	...
GJ 785	...	K2.0V	8.9	1997 Oct 19	3.73	...	8.3	9.3	10.3	11.3	13.3	14.3	14.3	i
GJ 1253	...	M5.0V	9.5	1998 Jan 7	8.27	10.1	12.1	13.6	15.1	16.1	17.1	18.1	18.1	...
GJ 791.2AB	AB	M4.5VJ	8.8	2002 Oct 28	7.67	10.3	12.3	13.3	14.3	15.3	17.3	18.3	18.3	b,c,d
GJ 793	...	M3.0V	8.0	1997 Aug 9	6.03	8.5	11.0	12.5	13.5	15.5	16.5	17.5	17.5	...
GJ 809	...	M0.0V	7.0	2003 Jul 2	4.92	7.8	9.8	10.8	11.8	12.8	14.8	15.8	16.8	d,i
GJ 820A	A	K5.0V	3.5	2002 Dec 3	2.54	9.3	10.3	11.3	13.3	14.3	15.3	b,d,i
GJ 820B	B	K7.0V	3.5	2002 Oct 16	2.89	7.3	8.3	9.3	11.3	12.3	14.3	15.3	15.3	b,d,i
GJ 827	...	F9.0V	9.2	1997 Aug 30	2.96	6.2	7.2	9.2	10.2	11.2	13.2	14.2	14.2	i
GJ 829AB	A/B	M3.0VJ	6.7	2002 Nov 17	5.74	9.4	10.9	11.9	12.9	13.9	15.9	16.9	16.9	b,c,d
GJ 831AB	A/B	M4.0VJ	7.9	2002 Oct 11	6.69	8.5	10.5	12.5	13.5	14.5	16.5	17.5	17.5	b,c

Table 2—Continued

Name	Resolved PSFs in FOV ¹	Spectral Type	Distance (pc)	Epoch	App. Mag. (<i>F180M</i>)	Absolute <i>F180M</i> Magnitude Limit								Notes
						0'2	0'4	0'6	0'8	1'0	2'0	3'0	4'0	
GJ 832	...	M1.5V	4.9	1997 Jul 28	4.60	8.5	10.5	11.5	12.5	14.5	15.5	16.5	16.5	...
G 188-38	...	M3.5V	8.9	1997 Oct 11	6.96	8.7	10.2	12.2	13.2	14.2	15.2	16.2	16.2	...
GJ 846	...	M3.5V	10.2	1997 Nov 17	5.36	8.0	9.0	11.0	12.0	13.0	14.0	15.0	16.0	g
LHS 3746	...	M3.5V	7.4	2002 Nov 18	6.79	9.6	10.6	11.6	13.6	14.6	16.6	17.6	17.6	...
GJ 845A	A	K4.0V	3.6	1997 Aug 4	2.17	10.2	11.2	12.2	14.2	16.2	16.2	b,i
GJ 849	...	M3.0V	8.9	1997 Nov 15	5.69	9.2	10.2	11.2	12.2	13.2	15.2	17.2	17.2	...
LHS 3799	...	M4.5V	7.4	1997 Oct 29	7.47	10.1	12.6	14.1	14.6	15.6	16.6	17.6	17.6	...
GJ 860A	A/B	M3.0V	4.0	1998 Nov 10	5.04	10.0	11.0	13.0	14.0	15.0	17.0	18.0	18.0	b,d
GJ 860B	A/B	M4.0V	4.0	1998 Nov 10	5.04	12.0	13.0	14.0	14.5	15.0	17.0	18.0	18.0	b,d,e
GJ 867AC	AC	M2.0VJ	8.6	2002 Nov 18	5.11	8.8	10.3	11.3	12.3	13.3	15.3	16.3	16.3	b,c,d,i
GJ 867B	B	M3.5V	8.6	1998 Aug 14	6.66	8.8	10.3	12.3	12.8	14.3	16.3	17.3	17.3	b
GJ 873	...	M3.5V	5.0	2002 Dec 24	5.55	8.5	10.5	12.5	13.5	14.5	16.5	17.5	18.5	...
GJ 876	...	M3.5V	4.6	1997 Dec 5	5.16	8.7	10.7	12.7	13.7	14.7	15.7	17.7	18.7	...
GJ 1276	...	DZ9+	8.5	1997 Sep 21	13.56	15.3	16.3	17.3	17.3	17.3	18.3	18.3	18.3	a
GJ 877	...	M2.5V	8.6	1997 Aug 29	5.94	8.3	10.3	11.3	12.3	13.3	16.3	17.3	17.3	...
GJ 880	...	M1.5V	6.8	2002 Oct 15	4.80	8.3	9.8	10.8	11.8	12.8	14.8	15.8	16.8	d,i
GJ 881	A	A4.0V	7.6	1998 Aug 6	0.94	5.6	6.6	7.6	8.6	10.6	11.6	a,b,d,i
GJ 884	...	K7.0V	8.2	1997 Dec 28	4.44	7.4	9.4	10.4	11.4	12.4	13.4	15.4	15.4	...
GJ 887	...	M1.0V	3.2	1997 Sep 11	3.45	7.4	9.9	11.4	12.9	14.4	15.4	17.4	17.4	...
GJ 892	...	K3.0V	6.5	1997 Sep 19	3.17	...	8.4	9.9	10.9	11.9	12.9	14.9	14.9	i
GJ 896A	A/B	M3.5V	6.2	2004 Jun 30	5.57	7.0	8.5	10.0	11.0	12.0	14.0	15.0	16.0	a,b
GJ 896B	A/B	M4.5V	6.2	2004 Jun 30	6.55	8.0	10.0	12.0	12.0	13.0	14.0	15.0	16.0	a,b
GJ 1286	...	M5.0V	7.2	1997 Sep 18	8.42	13.7	14.7	15.7	16.2	16.7	18.7	18.7	18.7	...
GJ 902	...	K3V	11.4	1997 Oct 19	4.56	7.7	8.7	10.7	11.7	11.7	13.7	14.7	15.7	g
GJ 905	...	M5.5V	3.1	2003 Jan 12	6.25	11.5	13.5	14.0	14.5	15.5	17.5	18.5	19.5	...
GJ 1289	...	M3.5V	8.1	1997 Sep 10	7.39	10.5	12.5	13.5	14.5	15.5	17.5	18.5	18.5	...
GJ 908	...	M1.0V	5.9	1997 Sep 9	5.13	9.6	10.6	12.1	13.1	14.1	16.1	17.1	17.1	...

¹A/B denotes that components A and B are resolved. AB denotes an unresolved known multiple.

^aNo PSF subtraction

^bKnown multiple system, excluding planets

^cSensitivity measured around unresolved or very close binary

^d2*MASS* *H* magnitude for primary

^eOff-center by more than 5''

^fSensitivity measured around brighter component only

^gBeyond 10 pc

^hSensitivity measurements exclude 30° between components.

ⁱSaturated core

Table 3. Background Sources with Companion-Like Colors

Primary	Separation	P. A. (deg)	Mimics	Deciding Factor
GJ 633	8''5	157.3	Late L in <i>F207M-F222M</i>	Too red to be late L in <i>F110W-F180M</i>
GJ 633	3''3	268.6	Late L in <i>F207M-F222M</i>	Too red to be late L in <i>F110W-F180M</i>
GJ 1093	8''0	250.6	Mid M in <i>F110W</i> colors	Background M1 or earlier in <i>F207M-F222M</i>
GJ 1224	12''6	91.4	Mid L in <i>F110W-F222M</i>	Background early M in <i>F180M-F222M</i>
GJ 367	8''4	3.3	Early L in <i>F180M-F207M</i>	Background main sequence in <i>F110W-F222M</i>
GJ 438	13''2	254.0	Hot white dwarf	Too red to be hot WD in <i>F110W-F180M</i>

Table 4. Astrometry of Unsaturated Resolved Systems

Pair	ρ (")	σ_ρ	P.A. (° E of N)	$\sigma_{P.A.}$	Epoch	Δ Magnitude			
						<i>F110W</i> ^a	<i>F180M</i>	<i>F207M</i>	<i>F222M</i>
GJ 1005AB	0.329	0.008	234.4	1.0	2002.7532	...	1.27	1.31	1.32
GJ 65AB	1.653	0.008	103.3	0.2	2002.8540	...	0.18	0.15	0.16
GJ 84AB ^b	0.443	0.006	103.4	1.0	2002.7506	4.59	4.01	4.18	3.82
GJ 105AC	3.220	0.036	293.5	0.4	1998.0225	5.96	5.87	5.45	5.40
LP 771-95AB	7.706	0.008	315.0	0.0	2003.4620	...	0.36	0.36	0.35
LP 771-95BC	1.344	0.008	138.1	0.2	2003.4620	...	0.56	0.54	0.50
GJ 169.1AB	9.201	0.008	63.7	0.0	2002.7693	...	5.89	5.98	6.07
GJ 229AB	7.627	0.031	164.1	0.1	1997.6202	9.63	11.44	9.44	10.75
GJ 257AB	0.560	0.008	280.4	0.6	1998.8271	...	0.03	0.00	0.00
GJ 1116AB	1.498	0.007	102.7	0.2	1998.8562	0.42	0.35	0.32	0.30
GJ 618AB	5.574	0.008	226.8	0.0	1998.7837	...	2.66	2.58	2.49
GJ 644A-BD	0.258	0.048	151.3	7.6	1998.7868	...	0.41	0.41	0.43
GJ 661AB	0.647	0.008	187.6	0.5	2002.6489	...	0.43	0.29	0.28
GJ 1230AC-B	5.117	0.008	6.1	0.0	2003.0605	...	1.91	1.88	1.85
GJ 747AB	0.234	0.048	87.4	8.4	2002.9441	...	0.02	0.05	0.03
GJ 1245AB	6.964	0.007	82.6	0.0	1998.7734	0.17	0.16	0.15	0.13
GJ 1245AC	0.594	0.007	269.6	0.5	1998.7734	1.49	1.29	1.18	1.08
GJ 860AB	3.184	0.008	99.5	0.1	1998.8590	...	1.01	0.97	0.94
GJ 896AB	5.351	0.008	87.9	0.0	2004.4956	...	1.54	1.48	1.43

^aMissing values correspond to stars with central core saturation for which a PSF fit is not available.

^bValues from G04, Table 4.

Table 5. M Dwarf Multiple Systems with Separations Between 5 and 70 AU Recovered in the Survey

A Component ^a	Spectral Type	M_H ^b	Mass ^c M_\odot	B Component	Spectral Type	M_H ^b	Mass ^c M_\odot	Angular Separation	Inferred Semi-major Axis (AU) ^f
GJ 229A	M1.5V	5.41	0.59	GJ 229B	T6.0	16.81	0.05: ^d	7''62	55.2
GJ 84A	M2.5V	5.95	0.52	GJ 84B	M7.0V	10.54	0.084 ^e	0''44	5.2
GJ 661A	M3.0V	6.03	0.51	GJ 661B	M3.0V	6.03	0.51	0''70	5.6
GJ 896A	M3.5V	6.60	0.39	GJ 896B	M4.5V	7.62	0.22	5''35	42.1
GJ 618A	M2.5V	6.62	0.38	GJ 618B	M4.5V	8.43	0.15	5''62	58.7
GJ 860A	M3.0V	7.02	0.31	GJ 860B	M4.0V	7.95	0.18	3''19	16.2
GJ 1230A	M4.0V	7.34	0.26	GJ 1230B	M5.0V	8.46	0.15	5''11	53.2
LP 771-95A	M2.5V	7.56	0.23	LP 771-95B	M3.5V	7.92	0.18	7''74	67.8
GJ 257A	M3.0V	7.63	0.22	GJ 257B	M3.0V	7.66	0.21	0''57	5.7
GJ 1245A	M5.5V	9.05	0.12	GJ 1245B	M6.0V	9.40	0.10	7''01	40.1
GJ 1116A	M5.5V	9.24	0.11	GJ 1116B	M6.0V	9.58	0.10	1''51	9.9
GJ 65A	M5.5V	9.32	0.11	GJ 65B	M6.0V	9.50	0.10	1''66	5.6

^aOrdered by decreasing mass, as shown in Figure 9.

^b H band photometry from *2MASS*. Close binaries were deconvolved adopting $\Delta H = \Delta F180M$.

^cBased on the Mass-Luminosity Relation of Henry & McCarthy (1993).

^dEstimate based on Allard et al. (1996).

^eG04

^fstatistically corrected for projection effects (Fischer & Marcy 1992).

Table 6. Summary of M Dwarf Multiplicity Fractions

Companion Range Spectral Type	Search Radius AU	Systems Probed	Detections	Hidden	Mult. Fraction %	Volume Limited?
M0V - M9V	5 - 70	126	11	2	$10.3^{+3.4}_{-2.1}$	Yes
L0 - L9	5 - 70	51	0	0	$0.0^{+3.5}_{-0.0}$	No
L0 - L9	12 - 70	126	0	0	$0.0^{+1.4}_{-0.0}$	Yes
L0 - T9	10 - 70	43	1	0	$2.3^{+5.0}_{-0.7}$	No
L0 - T9	14 - 70	126	1	0	$0.8^{+1.8}_{-0.2}$	Yes

Table 7. Brown Dwarf Masses (M_\odot) Based on Models of Chabrier et al. (2000).

	L3	L5	L8	T5	T7
T_{eff} ^a	2000	1750	1500	1200	900:
1 Gyr	0.070	0.060	0.050	0.050	0.030:
3 Gyr	0.073	0.070	0.057	0.052	0.040:
5 Gyr	0.075	0.072	0.065	0.065	0.050:

^aGolimowski et al. (2004a)